



Virtual Wind Tunnel

I2 Individual Report

Felix Browne

MEng Mechanical Engineering

2014

Supervisor: Dr Gavin Tabor

Abstract

Wind tunnels are used in industry to experimentally determine the aerodynamic characteristics of an object. Regarding the automotive sector, minimising aerodynamic drag is key to producing more efficient designs, increasing fuel efficiency and allowing industrial environmental standards to be met. This group project aimed to create a 'Virtual Wind Tunnel' combining concept car design, Computer Aided Design (CAD), Computational Fluid Dynamics (CFD) and experimental testing. The individual contribution to the project described herein aimed to design a concept car, conduct Reynolds-Averaged-Navier-Stokes (RANS) CFD analysis and produce scale models using Additive Layer Manufacture (ALM). The feasibility of integrating ALM into the automotive design process was also explored, involving numerical and Fluid-Structure Interaction and parametric Finite Element analysis of a 1:2 scale vehicle model.

From the comparison of RANS turbulence models it was concluded that the realizable k- ϵ and SST k- ω models were most suited to automotive flow analysis due to their ability to better compute boundary layer separation and adverse pressure gradients. The ALM process selected to produce the scale models was material jetting because it provided the best compromise between surface finish, geometrical accuracy and cost effectiveness. It was concluded that ALM was a viable method to be integrated into automotive design because it has the potential to increase design freedom and shorten project lead times. The main barrier to the integration of ALM is persuading industry to accept the change, therefore overcoming the tradition of using conventional techniques such as clay modelling. Recommended future work includes the design of a generic scale model chassis base, and investigating the thermal effects of wind tunnel testing on polymer structures. Also, the completion of a Return on Investment analysis for ALM processes is key before they can be adopted in an industrial role.

Keywords: Concept car, automotive design, Additive Layer Manufacture, Computational Fluid Dynamics.

Acknowledgements

I would like to express my thanks and gratitude to Dr Gavin Tabor for his continued support and guidance throughout the project. I would also like to thank Mr James Bradbury at the Centre for Additive Layer Manufacture (University of Exeter), for his advice and assistance in producing the concept car models presented herein. Finally I extend my thanks to Mr Adrian Gaylard at Jaguar Land Rover for his knowledge of industrial automotive design practices.

Contents

Abstract.....	i
Acknowledgements	ii
1. Introduction	1
1.1 Project Overview and Group Structure.....	1
1.2 Aims and Objectives	2
2. Background and Literature Review	3
2.1 Incompressible External Flow	3
2.2 Computational Fluid Dynamics	4
2.2.1 RANS Turbulence Models	4
2.2.1.1 Standard k- ϵ Model.....	5
2.2.1.2 Realizable k- ϵ Model.....	5
2.2.1.3 SST k- ω Model	5
2.2.1.4 Spalart-Allmaras Model	6
2.3 The Ahmed Body	6
2.4 Finite Element Analysis	7
2.5 Fluid-Structure Interaction.....	8
2.6 Automotive Design and Additive Layer Manufacture.....	9
2.6.1 Concept Car Design	9
2.6.2 Additive Layer Manufacture	10
2.6.3 Integration of ALM into Automotive Design	11
3. Methodology.....	13
3.1 Concept Car Design	13
3.1.1 Modified Ahmed Body.....	13
3.1.2 Concept Design and Analysis	13
3.2 Computational Fluid Dynamics Analysis	15
3.2.1 Case Setup and Meshing	15
3.2.2 Uniform Inlet Velocity Profile	17
3.2.3 Parabolic Inlet Velocity Profile	17
3.3 Finite Element Analysis	17
3.4 Fluid-Structure Interaction Analysis	18
3.5 Additive Layer Manufacture of Concept Car Models	18
4. Results and Discussion	20
4.1 Concept Car Analysis	20
4.1.1 Modified Ahmed Body.....	20
4.1.2 Initial Concept Analysis	22
4.1.3 Final Concept Analysis	22

4.1.3.1 Comparison of RANS Turbulence Models	23
4.1.3.2 Comparison between Uniform and Parabolic Inlet Velocity Profiles	24
4.2 Parametric Finite Element Analysis Study	25
4.3 Fluid-Structure Interaction Analysis	26
4.4 Additive Layer Manufacture of Scale Models	28
4.4.1 Comparison of ALM with Clay Modelling	29
5. Sustainability	31
6. Project Management	33
6.1 Budgeting	33
7. Conclusions	34
7.1 Summary	34
7.2 Recommendations for Future Work	34
References	35
Appendix A: User Defined Function for a Parabolic Inlet Velocity Profile	40
Appendix B: Health and Safety Risk Assessment	41
Appendix C: Final Gantt Chart	42

1. Introduction

The analysis of external fluid flow around objects is crucial to many industries, for example aerospace and automotive. Regarding the automotive sector concept cars undergo both numerical and experimental analysis in order to determine their aerodynamic characteristics. The drag forces acting on cars are of particular interest because of the industrial targets set upon improving fuel efficiency [1], therefore reducing carbon emissions.

Wind tunnels involve moving air around stationary objects for the purpose of experimental analysis, for example taking pressure and velocity readings. Drag forces are crucial for automotive vehicle testing, and can be measured using equipment such as a drag balance. Automotive scale models are traditionally constructed using clay modelling techniques, allowing very flexible design freedom. It is however a highly skilled, time consuming and labour intensive process. Additive Layer Manufacture (ALM) involves building up a component or model layer by layer typically using polymers such as acrylic. ALM has the potential to replace clay modelling, maintaining the design freedom and reducing project lead times by allowing models of design iterations to be rapidly produced for wind tunnel testing.

Computational Fluid Dynamics (CFD) analysis of automotive designs allows concepts to be tested numerically without the requirement for specialist equipment and large work spaces, therefore having the potential to save the high costs associated with wind tunnels. A disadvantage of CFD models however is that they provide a numerical approximation to the true output; therefore inaccuracies (largely dependent on the model used) are introduced. Reynolds-Averaged-Navier-Stokes (RANS) turbulence models provide relatively accurate results whilst requiring low computational resources, and have been used in the project presented herein.

The Virtual Wind Tunnel group project aimed to investigate aspects of automotive aerodynamic analysis combining concept car design, Computer Aided Design (CAD), CFD and experimental testing. The individual project described herein focussed on the feasibility of the integration of ALM into the automotive design process. This report will initially describe the aims, objectives and structure of the group project. Key concepts, including CFD and ALM, will be introduced and discussed in the form of a literature review. The methodology undertaken during the project will be outlined including the concept car design process, computational analysis and manufacture of the scale models. The results will then be presented and discussed, and a review into sustainability aspects (in particular social, environmental and economic impacts) will be provided.

1.1 Project Overview and Group Structure

The group was comprised of eight members and split into three sub-groups; the Automotive Design group, the High Performance Computing (HPC) group and the Experimental group. The Automotive Design group was concerned with the design, RANS analysis and ALM production of a concept car. The HPC group was tasked to conduct more accurate Large Eddy Simulation (LES) analysis whilst investigating meshing, design optimisation and urban canyon flow modelling. The Experimental group aimed to re-design and re-build the University of Exeter wind tunnel, and experimentally test the concept car model for comparison with the CFD results.

1.2 Aims and Objectives

The overall group aims, which were described in the group report G1 [2], are presented below. The associated deliverables for each aim are also provided as sub-points.

- To investigate the integrated design of a concept car combining CAD, CFD and experimental wind tunnel testing.
 - Design and manufacture a concept car using CAD and ALM.
 - Virtual rendering of the CAD concept car using Blender.
 - RANS CFD simulation of the concept car.
 - Experimental testing of the concept car in the University of Exeter wind tunnel.
- To use High Performance Computing to provide accurate CFD results.
 - Create a Virtual Wind Tunnel with a focus on importing, meshing, design optimisation and LES.
 - Investigate air flow profiles in an urban environment.
- To re-design and manufacture the University of Exeter's wind tunnel.
 - Design a new test chamber for the wind tunnel.
 - Manufacture the test chamber.

The main aims of the individual project presented in this report were to design a concept car external geometry, create scale models using ALM and explore the integration of ALM into the automotive design process. The individual objectives are outlined below.

- To analyse an initial basic car geometry and optimise a single feature (the rear slant angle).
- To design a concept car.
- To conduct RANS CFD analysis for the concept car, comparing turbulence models.
- To produce two scale models using ALM, including the final concept car and an earlier design iteration.
- To investigate the integration of ALM into the automotive design process.

2. Background and Literature Review

Knowledge of external incompressible flow, Computational Fluid Dynamics, Finite Element Analysis, Fluid-Structure Interaction and Additive Layer Manufacture is crucial to this project. In particular the concept of turbulence and boundary layers are important when understanding aerodynamic drag forces. A comprehensive review of these topics was discussed in Browne [3]. A summary of the key concepts are provided below.

2.1 Incompressible External Flow

At all but very high velocities the flow of air around an object can be assumed to be incompressible. The Reynolds number can be used to describe the state of a fluid flow. Generally for Reynolds numbers of less than 10^5 the flow is laminar, whilst greater than 5×10^5 corresponds to turbulent flow. A transition state exists between these values, where regions of both laminar and turbulent flow are present. Turbulent flow is comprised of eddies of varying magnitudes contributing to random, irregular motion. The Reynolds number can be calculated using Equation 1 [4] where U is the flow velocity, L is the characteristic length and ν is the kinematic viscosity of the fluid.

Equation 1: $Re = \frac{UL}{\nu}$

The region of fluid close to an immersed surface, and which suffers affected flow as a result of it, is known as a boundary layer. A velocity profile exists in the boundary layer between the free stream flow and the fluid in contact with the surface of the body, which has zero velocity. This is a result of decelerated flow due to surface shear forces opposing the fluid motion, known as the ‘no slip’ condition [5]. The diagram in Figure 1 [6] describes the formation of a turbulent boundary layer.

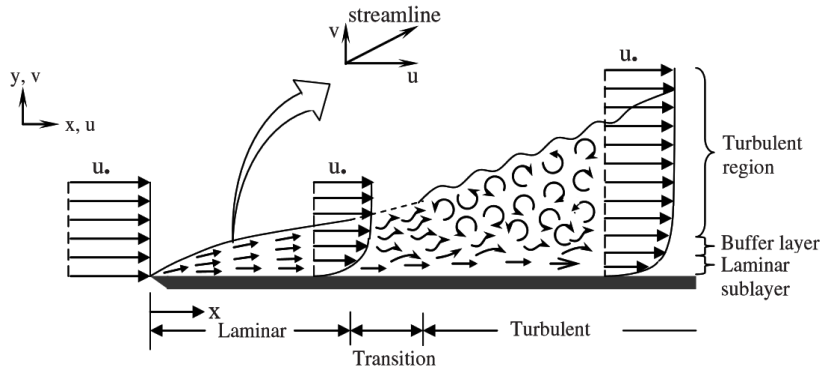


Figure 1: Diagram describing the formation of a turbulent boundary layer [6].

The boundary layer transitions from laminar to turbulent flow at a local Reynolds number equal to 10^5 [5]. For a flat plate, the thickness of the boundary layer (δ) with respect to the distance from the leading edge (x) is described by Equation 2 [5].

Equation 2: $\frac{\delta}{x} = \frac{0.376}{Re_x^{0.2}}$

The total drag experienced by a body submersed and in relatively motion with a fluid is the sum of the pressure and skin friction drag forces. The pressure drag is dependent upon the pressure forces acting on the body, whilst the skin friction drag is a result of the shear forces acting between the body and the fluid [5].

The wake region is the area of turbulent flow downstream of a body, consisting of large scale eddies with a high rate of energy dissipation [5]. This is due to boundary layer separation, which is a result of adverse pressure gradients and viscous forces acting on the surface. The area of low velocity at the front of an object, known as the stagnation point, produces a region of high pressure greater than the pressure at the rear of the submerged object. The pressure drag is therefore the resultant force of the pressure distribution.

A wider wake results in greater drag force. Drag can therefore be minimised by reducing the width of the wake through delaying or preventing boundary layer separation from the surface of the body [5]. Higher levels of turbulence generally results in earlier transition. The drag on a body can be calculated theoretically using Equation 3 [5], where C_D is the drag coefficient, ρ is the fluid density, U is the flow velocity and A is the projected area of the body.

Equation 3: $F_D = \frac{1}{2} C_D \rho U^2 A$

2.2 Computational Fluid Dynamics

Computational Fluid Dynamics (CFD) is a numerical approach to solving fluid flow problems using the Finite Volume method. Initially a mesh is created by dividing the flow domain into control volumes, known as cells [7]. A larger number of cells generally provides a closer numerical approximation to the actual solution, however also requires greater computing power and resources [7]. Fluid flow is governed by the Navier-Stokes equations. In the Finite Volume method the Navier-Stokes equations are integrated over each control volume and discretized to produce algebraic equations, which can be solved iteratively [8].

A variety of CFD models exist, however there is no turbulence model which can be applied to all forms of fluid flow problem. A compromise must therefore be made between the area of application, required accuracy of results and the computational resources available. RANS models, involving time averaged Navier-Stokes equations of motion and energy [9], were selected for use in this project because relatively accurate results can be obtained at low computational cost. A major disadvantage with the RANS model is the inability to predict unsteadiness on the wake region [10]. Another identified flaw is that RANS models can fail when predicting flow separation in largely separated flows [11].

A wide range of other numerical fluid flow analysis methods exist including Direct Numerical Simulation (DNS), Detached Eddy Simulation (DES) and LES [7]. Techniques such as LES can provide much more accurate numerical results, however they have been identified to be more computationally expensive than the RANS models by factors ranging from 10 to 100 [12]. Studies into hybrid RANS/LES models have also been identified [12, 13].

2.2.1 RANS Turbulence Models

For most of the analyses undertaken during this project the realizable $k-\epsilon$ model was used. For the analysis of the final concept car, the results of which are detailed in section 4.1.3, four different RANS turbulence models were compared. A background to the four models is provided below. It is worth noting that the transport equations shown include a density term (ρ) corresponding to compressible flow which was not considered in the studies undertaken in this project. A full list of the nomenclature corresponding to the transport equations provided in this section can be found in the *Fluent 6.3 User's Guide* [14].

2.2.1.1 Standard k-ε Model

The k-ε model is one of the most well established turbulence models, and focusses on the mechanisms affecting turbulent kinetic energy [7]. The standard k-ε model includes two equations (for k and ε respectively), which are used to define the velocity and length scales. Versteeg et al. [7] state that the standard k-ε model performs well in confined flows, however it has been known to perform poorly in unconfined flows with weak shear layers, rotating flows and flows with large extra strains. It is therefore not the best model for automotive external aerodynamics, which involves the modelling of largely separated flows and turbulent wakes. The turbulent dissipation energy (k) and the rate of dissipation (ε) are obtained from the transport equations shown in Equation 4 and Equation 5 [14] respectively.

$$\text{Equation 4: } \frac{\partial}{\partial t}(\rho k) + \frac{\partial}{\partial x_i}(\rho k u_i) = \frac{\partial}{\partial x_j} \left[\left(\mu + \frac{\mu_t}{\sigma_k} \right) \frac{\partial k}{\partial x_j} \right] + G_k + G_b - \rho \epsilon - Y_M + S_k$$

$$\text{Equation 5: } \frac{\partial}{\partial t}(\rho \epsilon) + \frac{\partial}{\partial x_i}(\rho \epsilon u_i) = \frac{\partial}{\partial x_j} \left[\left(\mu + \frac{\mu_t}{\sigma_\epsilon} \right) \frac{\partial \epsilon}{\partial x_j} \right] + C_{1\epsilon} \frac{\epsilon}{k} (G_k + C_{3\epsilon} G_b) - C_{2\epsilon} \rho \frac{\epsilon^2}{k} + S_\epsilon$$

2.2.1.2 Realizable k-ε Model

The realizable k-ε model has two main differences compared to the standard model: a new formulation for the turbulent viscosity and a new transport equation for the dissipation rate derived from the mean-square vorticity fluctuation equation [14]. Constraints are applied to the Reynolds stresses, providing better performance for flows involving boundary layers with separation and adverse pressure gradients. An identified limitation of the realizable k-ε model is that turbulent viscosities can be produced in a domain containing both rotating and stationary fluid zones, for example multiple reference frames [14]. Equation 6 and Equation 7 [14] provide the transport equations for k and ε respectively.

$$\text{Equation 6: } \frac{\partial}{\partial t}(\rho k) + \frac{\partial}{\partial x_i}(\rho k u_i) = \frac{\partial}{\partial x_j} \left[\left(\mu + \frac{\mu_t}{\sigma_k} \right) \frac{\partial k}{\partial x_j} \right] + G_k + G_b - \rho \epsilon - Y_M + S_k$$

$$\text{Equation 7: } \frac{\partial}{\partial t}(\rho \epsilon) + \frac{\partial}{\partial x_i}(\rho \epsilon u_i) = \frac{\partial}{\partial x_j} \left[\left(\mu + \frac{\mu_t}{\sigma_\epsilon} \right) \frac{\partial \epsilon}{\partial x_j} \right] + \rho C_{1\epsilon} S_\epsilon - \rho C_{2\epsilon} \frac{\epsilon^2}{k + \sqrt{\nu \epsilon}} + C_{1\epsilon} \frac{\epsilon}{k} C_{3\epsilon} G_b + S_\epsilon$$

The k equation is the same as the standard and RNG models (other than the constants), however the ε equation is different. The production term ($\rho C_{1\epsilon} S_\epsilon$) does not include the production of k, which is said to better represent the spectral energy transfer [14].

2.2.1.3 SST k-ω Model

The SST k-ω model was created as a hybrid using the k-ε model in the fully turbulent region away from the wall, and a transformation of the k-ω into the k-ε model in near-wall regions by substituting $\epsilon = k\omega$ into the ε equation [7]. Versteeg et al. [7] summarise the main improvements to be revised model constants; the introduction of blending functions to achieve a smoother transition between models through the reduction of numerical instabilities; and the limiting of the eddy viscosity in order to improve performance with wakes and adverse pressure gradients. The transport equations are provided in Equation 8 and Equation 9 [14].

$$\text{Equation 8: } \frac{\partial}{\partial t}(\rho k) + \frac{\partial}{\partial x_i}(\rho k u_i) = \frac{\partial}{\partial x_j} \left(\Gamma_k \frac{\partial k}{\partial x_j} \right) + \tilde{G}_k - Y_k + S_k$$

$$\text{Equation 9: } \frac{\partial}{\partial t}(\rho \omega) + \frac{\partial}{\partial x_i}(\rho \omega u_i) = \frac{\partial}{\partial x_j} \left(\Gamma_\omega \frac{\partial \omega}{\partial x_j} \right) + G_\omega - Y_\omega + D_\omega + S_\omega$$

2.2.1.4 Spalart-Allmaras Model

The Spalart-Allmaras model involves a single transport equation for the kinematic eddy viscosity parameter [7]. Whilst the k- ϵ model computes a length scale through the combination of the transport properties (k and ϵ), the one equation Spalart-Allmaras model requires a length scale to be specified. Versteeg et al. [7] state that it is particularly suited to aerofoil analysis due to its good performance for boundary layers with adverse pressure gradients. Disadvantages include reduced sensitivity to transport processes in rapidly changing flows, and the length scale is difficult to define for complex geometries, making it less suited to internal flows [7]. The transport equation is provided in Equation 10 [14].

$$\text{Equation 10: } \frac{\partial}{\partial t}(\rho \tilde{\nu}) + \frac{\partial}{\partial x_i}(\rho \tilde{\nu} u_i) = G_{\tilde{\nu}} + \frac{1}{\sigma_{\tilde{\nu}}} \left[\frac{\partial}{\partial x_j} \left\{ (\mu + \rho \tilde{\nu}) \frac{\partial \tilde{\nu}}{\partial x_j} \right\} + C_{b2} \rho \left(\frac{\partial \tilde{\nu}}{\partial x_j} \right)^2 \right] - Y_{\tilde{\nu}} + S_{\tilde{\nu}}$$

2.3 The Ahmed Body

The Ahmed body represents a simplified car geometry. The model was first suggested by Ahmed et al. [15], and incorporates many features of automotive flow including displacement around the nose, uniform flow around the middle section and separation at the rear [8]. Figure 2 [16] provides a diagram of the Ahmed body with associated dimensions.

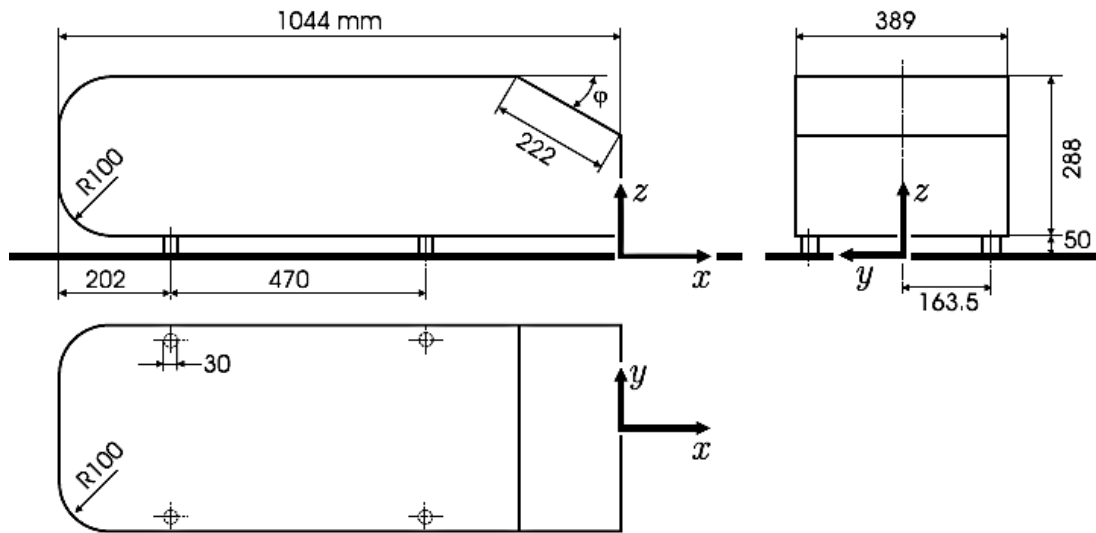


Figure 2: Diagram of the Ahmed body [16].

The angle of the rear slant is of particular interest because it determines the wake behind the body, which is the main contributor to the drag force [17]. Viscous drag effects were found to arise mostly from the lateral parts of the Ahmed body [18]. It has been determined that two critical angles exist, equal to 12.5 and 30 degrees [11], between which flow becomes separated and above which flow is fully detached. Maximum drag occurs at an angle of 30 degrees. The graph in Figure 3 [19] describes the relationship between the drag coefficient and rear slant angle.

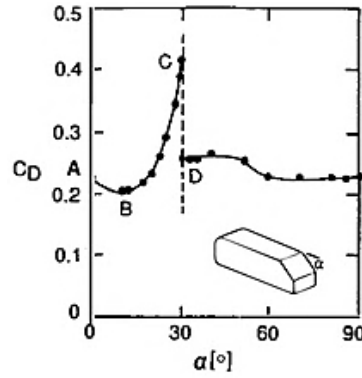


Figure 3: Graph of C_D against the rear slant angle for the Ahmed body [19].

The Ahmed body has been widely validated using a variety of techniques including LES [16, 18, 20], DES [21], RANS modelling [10, 17, 22, 23] and experimental testing [22, 24, 25]. It was therefore considered to be a good starting point for the concept car design in this project.

2.4 Finite Element Analysis

The Finite Element Analysis (FEA) method can be applied to a wide range of physical problems including structural, torsion, vibration, non-linear and steady state heat transfer analysis [26]. In this project the FEA method was applied in order to determine the deflections and stresses within a scale model initially loaded under its own weight, and later by an aerodynamic pressure load in an FSI analysis.

The FEA numerical method is relatively similar to the Finite Volume method (described in section 2.2). Ramamurty [26] states that the formulation of a finite element solution can be divided into several steps, which are outlined in this section. The initial stage is discretisation, where the computational domain is divided into sub-shapes called elements. The elements are connected by nodes, at which points unknown variables such as displacements or temperatures are to be determined. Dividing a geometry into elements provides an approximation to the actual solution, therefore an error will be introduced [27]. The accuracy of the solution can be improved by carrying out a mesh refinement study, where the number of elements is increased until the solution converges.

Following this the unknown variables are defined by polynomial expressions. The element equations are then derived by minimising an integral expression (known as a functional) with respect to the relevant nodal variables [26]. For structural mechanics the potential energy expression is written in integral form, and subsequently minimised with respect to nodal displacements. Element equations can be formulated either through variation formulation using calculus variation, or by weighted residual methods [26]. Matrices are then assembled to form global equations. Specifically, assembling all of the element equations generates the stiffness matrix and force vector for the global system. Equation 11 and Equation 12 [26] describe the equation formulation process where $[K^{(e)}]$ is the element stiffness matrix, $\{q^{(e)}\}$ is the element nodal displacement vector and $\{F^{(e)}\}$ is the element load vector.

$$\text{Equation 11: } [K^{(e)}]\{q^{(e)}\} = \{F^{(e)}\}$$

$$\text{Equation 12: } \sum_{e=1}^n ([K^{(e)}]\{q^{(e)}\} - \{F^{(e)}\}) = 0$$

Solving the global equations will provide a solution for the unknown variable, for example nodal displacements. Secondary quantities such as stresses and strains can be calculated when the nodal displacements are known. Equation 13 [26] describes the relationship between the global nodal displacement $\{Q\}$, force vector $\{F\}$ and global stiffness matrix $[K]$.

$$\text{Equation 13: } \{Q\} = [K]^{-1}\{F\}$$

Another technique is the equilibrium method, where the stress field variable and displacement are to be derived from the stress, and compatibility equations need to be satisfied [26]. Alternatively, the mixed method involves part of the domain being solved using displacement formulation and the rest using the equilibrium method. The diagram in Figure 4 [26] describes the normal and shear stresses acting on an element.

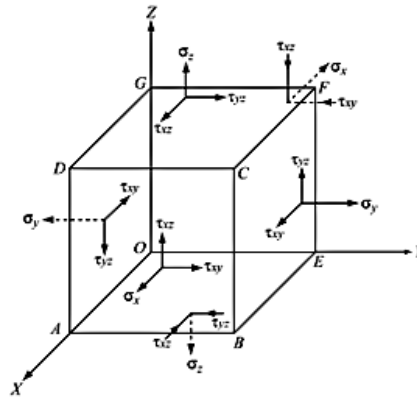


Figure 4: Diagram describing the normal and shear stresses on an element [26].

2.5 Fluid-Structure Interaction

Fluid-Structure Interaction (FSI) is a numerical method of combining fluid flow and structural analysis, and has been applied across a wide range of applications including simulating sloshing in a fuel tank [28]. FSI analyses are either one-way or two-way. The one-way analysis assumes that the deformation of the structure is not great enough to have a significant impact upon the fluid flow. In the two-way analysis the deformation of the solid is taken into account and updates the fluid flow analysis. An example of a two-way FSI analysis is the modelling of a morphing wind turbine blade described by Krawczyk et al. [29] utilising Ansys CFX and Mechanical software. The flow diagram in Figure 5 [29] effectively describes the two-way FSI process.

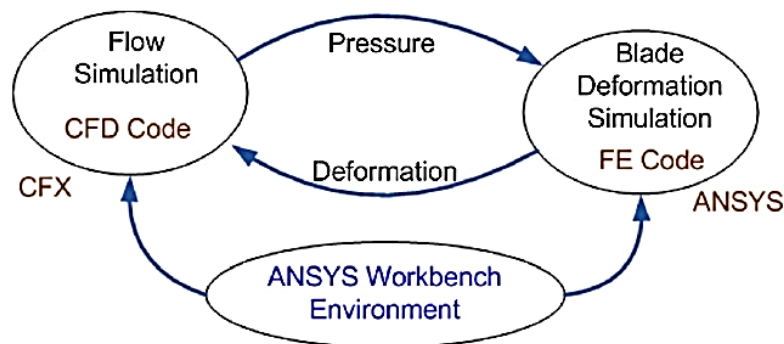


Figure 5: Diagram of a two-way FSI analysis process [29].

A wide range of different analysis techniques exist. Generally they can be characterised as either monolithic or partitioned approaches [30]. The monolithic approach provides better accuracy at a greater computational expense, and treats the model as a single system. The partitioned approach on the other hand, which solves the fluid and structure as separate systems, is less efficient. Meshing is another key aspect of FSI analysis. Hou et al. [30] propose that meshes are classified as either non-conforming (uniform), or conforming (non-uniform) meshes.

Many numerical models can be applied to FSI problems. An example of a conventional approach is the Arbitrary Lagrangian-Eulerian (ALE) method, which simulates the interface between the solid and fluid using body conforming grids, however performs poorly for problems involving large deformations [31]. The Immersed Boundary (IB) method, which includes both diffused interface and sharp interface methods, is often a quicker and cheaper process because it does not require dynamic re-meshing [31]. The Immersed Structural Potential Method is an update of the IB method, modelling the solid by a strain energy function and defining the FSI force by the spatial gradient in the Navier-Stokes equations [32]. The deformations are then calculated through interpolating kernel functions rather than using a finite element mesh.

The final technique to be explored in this review is the Immersed Finite Element Method. Improvements to the model have been described by Hesch et al. [33], including accounting for the deformation of a solid with a varying volume. Further improvements include the reduction of locking effects for isochoric deformations (achieved by updating the incompressibility constraints), and enhancing the robustness of the model by combining an implicit one-step time integration scheme and a Newton-Raphson linearisation strategy [33].

It was decided that the method to be employed in this project was one-way FSI, because the problem involved a stationary solid object immersed in a steady state fluid flow, and it was assumed that the deflections would not be significant enough to affect the fluid flow. One-way FSI is also relatively computationally inexpensive.

2.6 Automotive Design and Additive Layer Manufacture

ALM involves building up a component or model layer by layer, and has the potential to replace traditional clay modelling techniques in the automotive industry. A detailed overview of rapid prototyping was provided in Browne [3]. This section introduces a conventional concept car design process, and provides a summary of ALM.

2.6.1 Concept Car Design

This paragraph introduces an industrial automotive design process, described by Gaylard [34]. Generally models, often at scales of 1:4 or 1:2, are created using clay. A generic chassis is typically used as a base, followed by the addition of clay to produce the external car geometry. During the initial stages of the process there is a focus on aesthetics, and the models are worked on primarily by designers rather than engineers. Once a latter clay model has been created (following several design iterations) it is scanned and reverse engineered, producing a CAD model. The resultant CAD model can then be used for computational analysis such as CFD simulations.

2.6.2 Additive Layer Manufacture

ALM methods can be categorised by the way the material is processed, for example powder bed, material deposition and liquid curing. A series of generic process steps to ALM have been identified [35], and are described in this section. Initially a CAD model of the required geometry is created and converted to a Stereo Lithography (STL) file. During the conversion surfaces are triangulated and meshed, where the individual facets are defined through assigning normal vectors and a list of vertices [36, 37]. The approximate nature of the process requires a tolerance level to be set. Errors include overlapped or suspended edges and faces [38]. Following the conversion, the STL file is sliced into layers before printing. Proposed methods involving the direct slicing of CAD formats have also been investigated [38, 39]. Figure 6 displays a diagram showing the principle of tessellation [39].

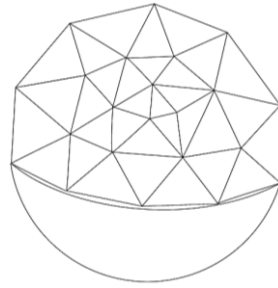


Figure 6: Diagram showing the principle of tessellation [39].

The STL file is then transferred to the ALM machine and printed. Once the process is complete the part is left to cool, and any support structures are removed. Post-processing is usually applied before the final application, for example surface finishing and treatment.

Three ALM processes were available for use at the University of Exeter Centre for Additive Layer Manufacture (CALM): laser sintering, material extrusion and material jetting. During the laser sintering process a powdered material is sintered and fused by a laser, forming the layer. Additional powder is then deposited upon the initial layer, and the process repeated until the entire geometry has been built up. Advantages of laser sintering include minimal waste, as unused powder can be recycled, and a wide range of materials can be used [40]. No support structures are required, therefore post-processing is also minimised. Figure 7 [41] displays a diagram describing the laser sintering process.

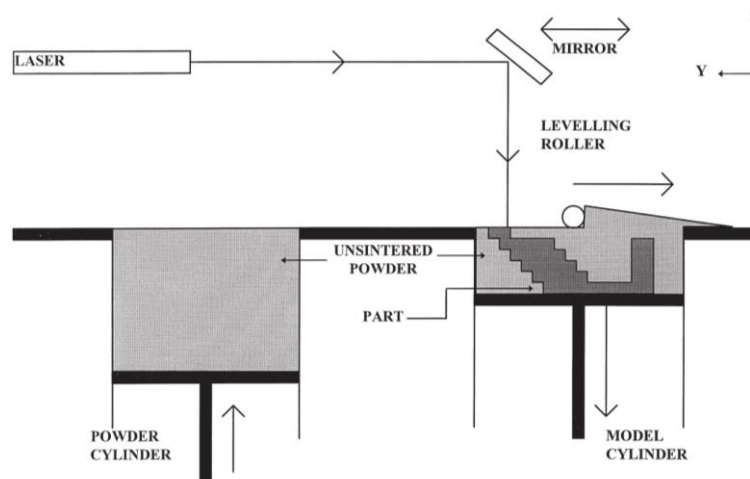


Figure 7: Diagram describing the laser sintering process [41].

Both the material jetting and material extrusion techniques are types of Fused Deposition Modelling (FDM). This process involves extruding a polymer filament through an extrusion head, where it is melted and deposited onto the part, thermally bonding the layers. A drawback is that FDM processes are limited to thermoplastics such as ABS and nylon, and require support structures [40, 42]. The diagram in Figure 8 [41] describes the FDM process.

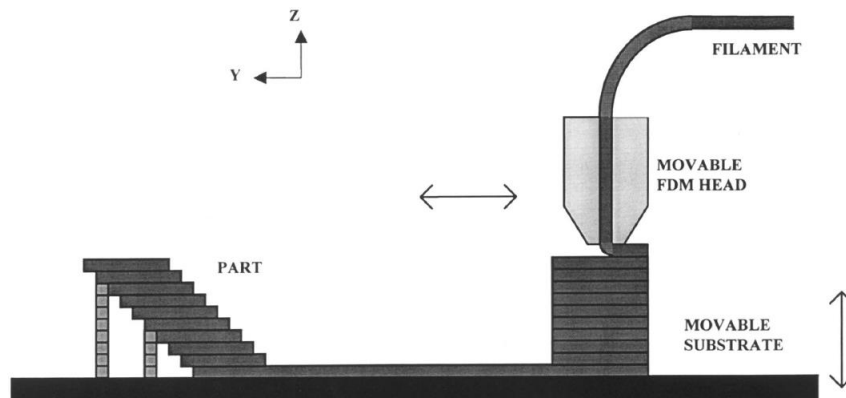


Figure 8: Diagram describing the FDM process [41].

2.6.3 Integration of ALM into Automotive Design

The relatively rapid nature of ALM means that concept car models could be produced quickly from CAD models during the design stage, allowing for experimental testing in a wind tunnel. The flow diagram in Figure 9 [3] describes the potential integration of ALM into the design process.

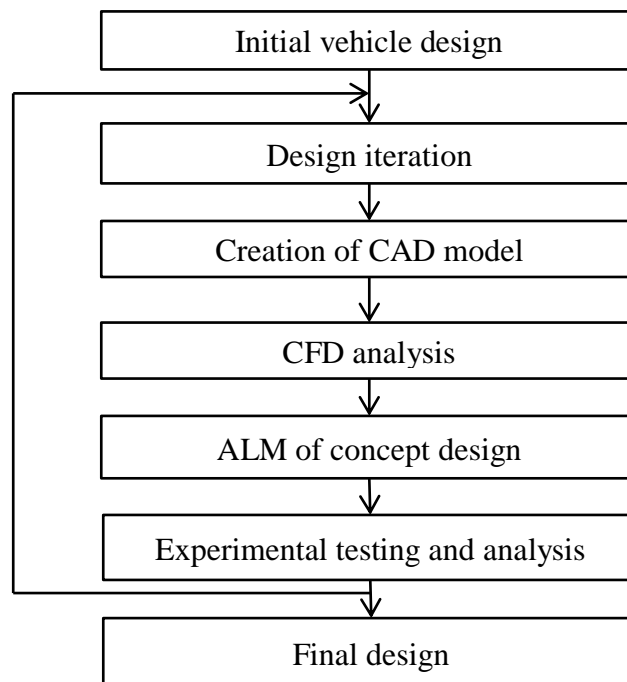


Figure 9: Flow diagram of an ALM integrated design process [3].

ALM has already been introduced to automotive applications in several ways. A 1:10 scale model of a sports car has been created using Selective Laser Sintering (SLS) for aesthetic design purposes [43]. More relevantly, a car model of dimensions 120x45x40cm has been

produced from gypsum and epoxy resin for wind tunnel testing [44]. The model was produced in sections, before being assembled by hand. A photograph of the model is shown in Figure 10 [44].

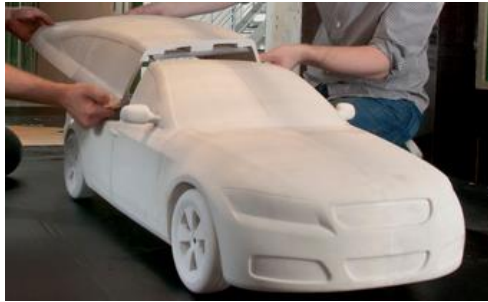


Figure 10: Picture of a 3D printed car model being assembled [44].

A potential issue arising from the ALM of large scale concept cars, for example 1:2 or 1:1, is the ability of the equipment to print the required size. Theoretically a part of almost any scale could be printed, provided that the equipment apparatus is of adequate proportions. The building of a custom large scale printing machine could however incur a very large initial cost before production can even begin. Relatively large scale printers do exist, for example the Voxeljet VX4000 [45], which provides a build space of 4x2x1m. This scale could comfortably produce a 1:2 scale automobile model. The same company has previously manufactured a model of an Aston Martin car at a scale of 1:3 from 18 pieces for film production [46]. The overall model had dimensions of 1480x620x270mm, and a build time of 25 hours. Photographs of the model are displayed in Figure 11 [46].



Figure 11: Photographs of the 3D printed Aston Martin car model [46].

Future developments to emerge in China include a 3D printer which will be able to manufacture metal parts 6m in diameter [47]. A printer of this scale could easily print a full scale automobile body if required. Cost is an important factor to be considered, and an investment analysis would need to be carried out to determine whether it would be more cost effective for a company to purchase the equipment or have models produced externally.

3. Methodology

This section will detail the methods used to carry out the project work including the design of the concept car, computational analysis (CFD, FEA and FSI) and the production of a scale model using ALM. SolidWorks [48] software was utilised for the CAD models and FEA in this project, whilst the fluid flow and FSI analyses were carried out using Ansys Workbench [49].

3.1 Concept Car Design

3.1.1 Modified Ahmed Body

The Ahmed body, introduced in section 2.3, incorporates many important features of automotive flow including flow separation at the rear. To provide a more realistic vehicle design for the initial study, the Ahmed body geometry was altered to include a bonnet. Figure 12 displays both the initial and modified Ahmed body geometries.

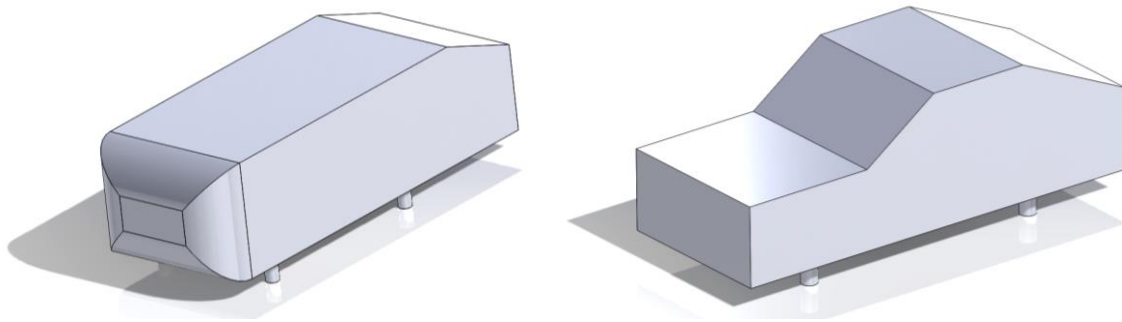


Figure 12: Initial (left) and modified (right) Ahmed body models.

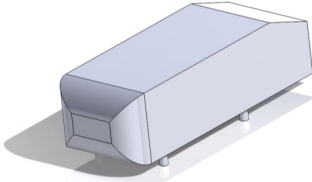
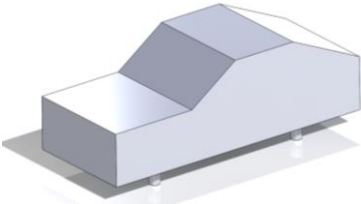
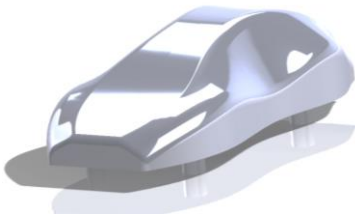
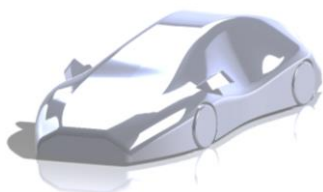
A parametric study was undertaken to investigate the effect of varying the rear slant angle, which has a large effect on the flow in the wake (the main contributor to the drag force). The rear slant angle was varied from 25° to 35° in increments of 2.5° , and CFD analysis was conducted using the methodology described in sections 3.2.1 and 3.2.2. The results of the study are discussed in section 4.1.1.

3.1.2 Concept Design and Analysis

The aim of this project was not to design a new car to be brought to market, but rather to create a new external car geometry containing key automobile vehicle features in order to investigate the various aspects of numerical analysis, model construction and experimental work. The results of the modified Ahmed body analysis (described in section 4.1.1) showed that maximum drag occurred at a rear slant angle of approximately 32.5° . Other studies undertaken in the Virtual Wind Tunnel project by Nima [50] and Crinion [51] concluded that the drag was minimised by including rounded fillets rather than sharp corners, and by reducing the angle of the front windscreen with respect to the horizontal.

The first iteration of the concept represented a combination of a new car body profile and the modified Ahmed body by using legs rather than wheels, and omitting complexities such as wing mirrors. To minimise the drag coefficient, a rear angle of approximately 25° degrees was chosen, sharp corners were avoided and the windscreen angle was made as shallow as possible. The final concept car design better represents a true car geometry, and was created by taking the body profile of the initial concept and adding wheels, wing mirrors and a rear diffuser. Table 1 summarises the evolution of the concept car from the Ahmed body. A larger picture of the final concept CAD model is provided in section 4.1.3.

Table 1: Summary of the concept car design evolution.

Concept Car	Description
	<ul style="list-style-type: none"> Initial simplified vehicle geometry (Ahmed body). Maximum drag identified to be at a rear slant angle of 30 degrees [11].
	<ul style="list-style-type: none"> Modified Ahmed body. Bonnet and windscreen added to provide more realistic geometry. Maximum drag found to occur at rear slant of 32.5 degrees. Drag found to be reduced by filleting sharp corners [50] and decreasing the angle of the windscreen [51].
	<ul style="list-style-type: none"> Design iteration. New body profile with rear slant angle of approximately 25 degrees, shallow windscreen angle and no sharp corners to reduce drag. Combined new body profile with modified Ahmed body – omitted complex external features.
	<ul style="list-style-type: none"> Final Design. New, complex body profile combined with external details including wheels, wing mirrors and a rear diffuser.

RANS CFD analysis of both the initial and final concept car designs were carried out as described in sections 3.2.1 and 3.2.2. To simplify the meshing process of the final concept design the wing mirrors and diffuser were removed. In order to compare their effectiveness, several RANS turbulence models were used for the final concept car analysis. The models included the standard k- ϵ , the realizable k- ϵ , the SST k- ω and the Spalart-Allmaras models, introduced in section 2.2.1. To provide an effective comparison the mesh was kept constant for each analysis. The results of the concept CFD analysis are presented in sections 4.1.2 and 4.1.3.

A study into the air flow within an urban environment (specifically Exeter High Street) was undertaken by Walton [52] as part of the Virtual Wind Tunnel group project. A two-dimensional CFD analysis of a full scale vehicle (of total length 4m) was therefore conducted. The aim of the analysis was to compare the flow effects of a realistic parabolic inlet velocity condition, provided by Walton [52], with a uniform inlet velocity of 10ms^{-1} (corresponding to a Reynolds number of 2.67×10^6). The analysis methodology is described in section 3.2.3.

3.2 Computational Fluid Dynamics Analysis

3.2.1 Case Setup and Meshing

This section details the generic fluid flow analysis methodology undertaken for the various cases presented in this report. Initially a model of the geometry was created using SolidWorks. The geometry was imported directly into Ansys, and an air domain was created by inserting an enclosure around the solid body. The enclosure was chosen to have dimensions of $8L \times L \times 2L$ with a length of $2L$ in front of the vehicle, where L is the length of the car body. This allowed the flow profile to fully develop, in particular downstream of the vehicle [18].

A Boolean operation was then used to subtract the car body from the air. Symmetry conditions were applied to the central vertical plane through the car body, greatly reducing the computational expense of the simulations. Symmetry conditions were also applied to the side and top faces of the enclosure in order to simulate an open air domain. Stationary wall conditions were assigned to the surface of the road and walls of the car body, whilst the inlet and outlet were defined as ‘velocity-inlet’ and ‘pressure-outlet’ respectively. Figure 13 displays the computational domain with symmetry conditions.

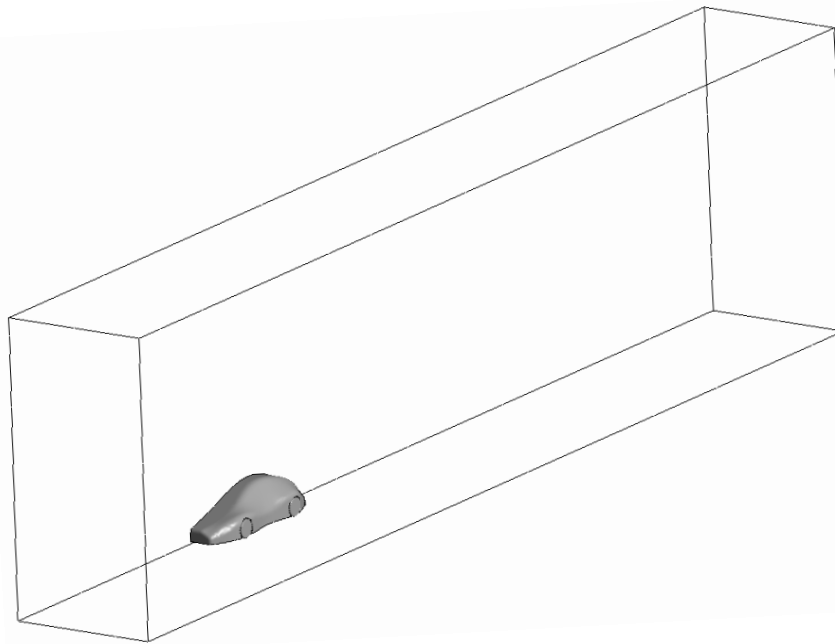


Figure 13: Diagram of the computational domain.

The mesh was generated using the meshing tool in Ansys Fluent. The cells not near to the car body were made large, preserving the overall number of cells and lowering the computational cost of the simulation. First Aspect Ratio program controlled inflation was applied to the walls of the car body, which was required to better capture the boundary layer [10]. A mesh refinement was then created around the car body at a distance $L/2$ above and to the side and L to the rear, covering the wake region [11, 53]. Figure 14 shows a side profile of the mesh from the analysis of the modified Ahmed body to demonstrate the wake region refinement.

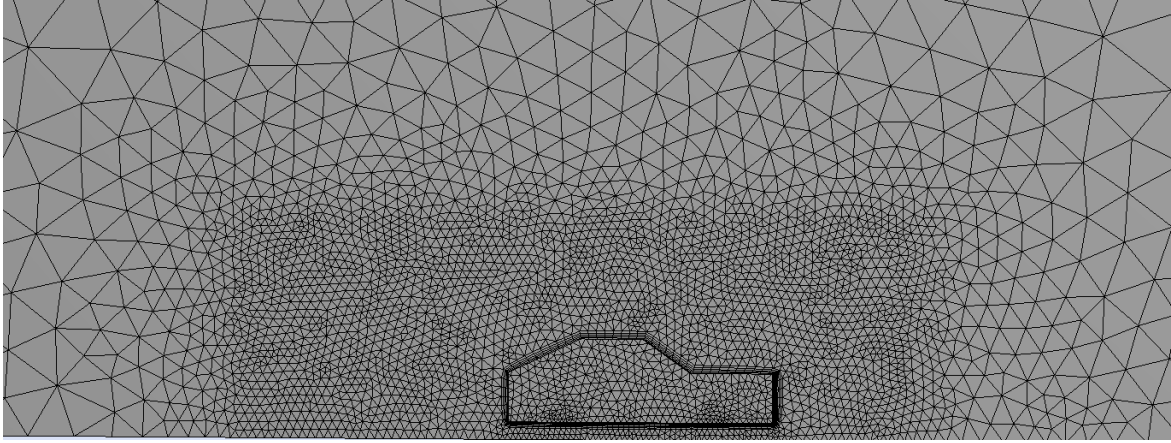


Figure 14: Side profile of the modified Ahmed body mesh.

In order to ensure accurate results were obtained a mesh refinement study was carried out for each CFD analysis, where the number of elements was increased until the output converged. The mesh refinement study for the modified Ahmed body with a rear slant angle of 25 degrees (introduced in section 3.1.1) is displayed in Figure 15 as an example.

Graph of C_D against Number of Elements

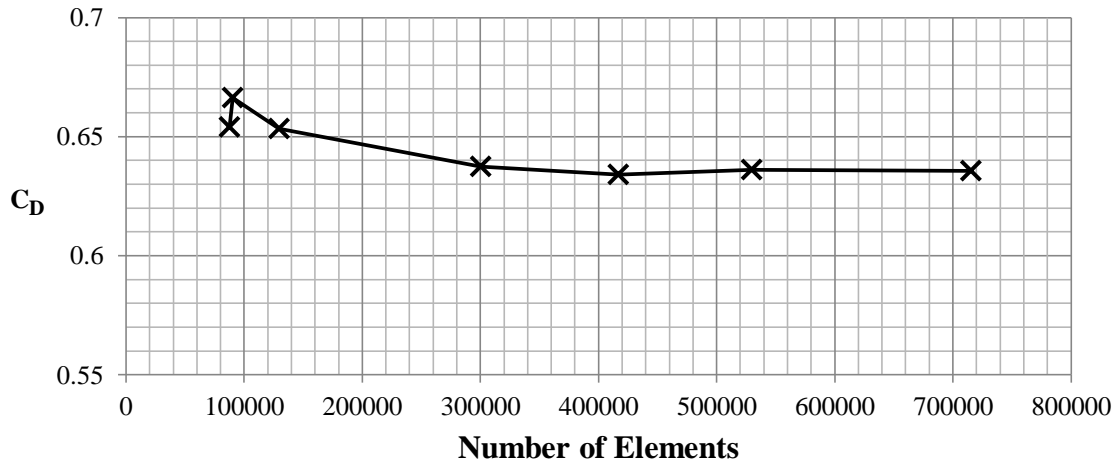


Figure 15: Mesh refinement study for the modified Ahmed body analysis.

Non-Equilibrium Wall Functions were applied to the model, which are recommended when dealing with complex flows involving separation, reattachment and pressure gradients [54]. Non-Equilibrium Wall Functions are sensitised to pressure gradients and account for local variation in the thickness of the viscous sub-layer when calculating the turbulent kinetic energy in wall adjacent cells [53]. The residual tolerance was set to a value of 10^{-3} , and the quality of the mesh was assessed by reporting the cell skewness and aspect ratio. A good mesh was crucial because low quality elements could incur inaccuracies downstream and affect the convergence of the residuals. Where issues with the convergence arose mesh properties such as the refinement level, smoothing and growth rate were altered. As part of the Virtual Wind Tunnel group project, further studies into meshing and residual convergence were undertaken by Nima [50] and Hamilton [55]. The drag coefficients were determined by reporting the drag force and project areas, and substituting them into Equation 3 (section 2.1).

3.2.2 Uniform Inlet Velocity Profile

For the majority of analyses undertaken in this project a uniform inlet velocity condition was set. An inlet velocity of 45ms^{-1} was specified when simulating the three-dimensional concept cars during the design process and FSI analysis, corresponding to the maximum air velocity the University of Exeter wind tunnel could produce. Using Equation 1 (provided in section 2.1) the Reynolds number of the flow over the concept cars (scaled down so they would theoretically fit into the University of Exeter wind tunnel) was calculated to equal 4.5×10^5 . This corresponded to turbulent flow; therefore RANS turbulence models were used. The Semi-Implicit Method for Pressure-Linked Equations (SIMPLE) scheme was utilised because the cases involved steady state flow.

3.2.3 Parabolic Inlet Velocity Profile

The velocity profile describing the flow through an urban environment was provided in the form of a polynomial function, presented in Equation 14 [52] and the graph in Figure 16. The lower and upper bounds of the profile were 0m and 2.7m respectively.

Equation 14:

$$U_x(y) = [0.506y^6 - 5.0841y^5 + 17.562y^4 - 22.423y^3 + 0.0843y^2 + 16.885y + 4.4157]_0^{2.7}$$

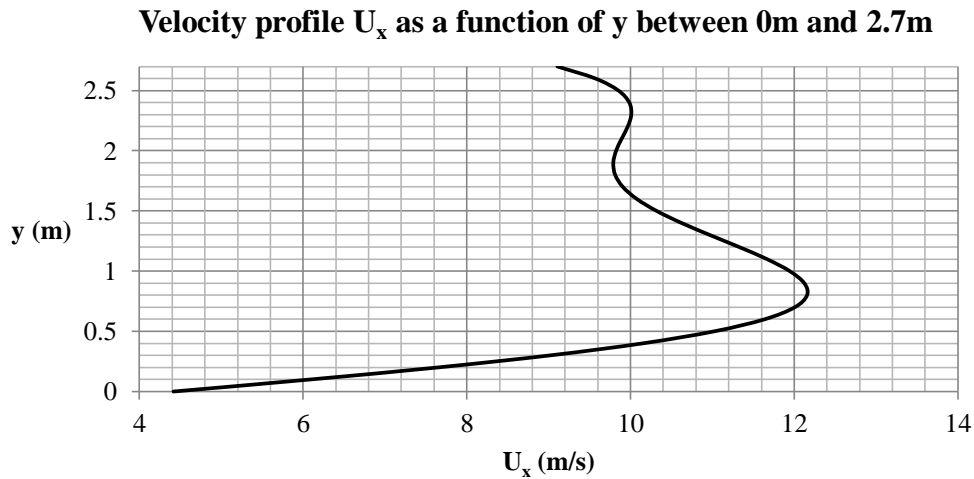


Figure 16: Graph of the velocity profile U_x as a function of y .

To set a non-uniform velocity profile at the domain inlet a User Defined Function (UDF) was compiled in the form of a C source code script. A loop written into the code allowed the parabolic velocity profile to be interpreted by Ansys Fluent by calculating the velocity at the centroids of all cell faces at the inlet [56]. The UDF script is provided in Appendix A.

3.3 Finite Element Analysis

In order to investigate the structural strength and mechanical characteristics of large scale ALM concept car models a parametric FEA design study was conducted. The purpose of the analysis was to determine the behaviour of a hollow model loaded under its own weight. For simplicity the initial concept car design, shown in section 3.1.2, was chosen. The shell thickness of the model was varied from 4mm to 20mm in increments of 2mm. Table 2 provides the material properties of acrylic [57] used in the analysis, corresponding to the material jetting process discussed in section 3.5. For comparison purposes, the material properties of nylon 12 [58] (corresponding to the laser sintering process) and ABS

[59] (material extrusion) are also provided. The ALM processes are further discussed in section 3.5.

Table 2: Material properties for acrylic [57], nylon 12 [58] and ABS [59].

Material	Density (kgm^{-3})	Tensile Strength (MPa)	Tensile Modulus (MPa)
Acrylic	1020	42.4	1283
Nylon 12	930	48	1650
ABS	1400	36	2265

The bottoms of the wheels on the model were given fixed displacement boundary conditions, and a gravity load was applied to the body. The design study was set up to minimise the Von Mises stress and maximum deflection whilst minimising the mass. Similar to the CFD analysis, a mesh refinement study was carried out to ensure that an appropriate mesh was used, therefore providing accurate solution data. The results of the parametric analysis are presented in section 4.2.

3.4 Fluid-Structure Interaction Analysis

A one-way FSI analysis was carried out to determine the effect of aerodynamic loading on a hollow ALM concept car scale model, simulating it in a wind tunnel. The geometry analysed was the output of the FEA design study which provided the best compromise between the mass and maximum deflection (a shell thickness of 8mm), which is justified in section 4.2. Initially a steady state CFD analysis was conducted using the method described in sections 3.2.1 and 3.2.2. The geometry file was then linked to the Ansys Static Structural solver. The diagram in Figure 17 highlights the links between the imported CAD file, fluid flow and static structural solvers in Ansys Workbench.

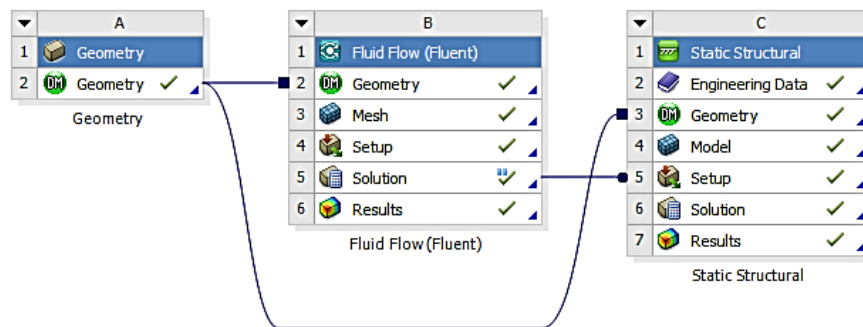


Figure 17: Diagram showing the links between the imported CAD file, fluid flow and structural analysis in Ansys Workbench.

To conduct the structural analysis the air domain around the car was suppressed, and a mesh of the solid geometry was created using the Mechanical meshing tool. Similar to the parametric structural analysis, described in section 3.3, the bottom of the wheels were assigned fixed displacement boundary conditions. A pressure load was imported from the CFD simulation to the surface of the car body, and the model was solved to determine the Von Mises stress and maximum deflection. The results of the FSI analysis, including stress and deflection plots, are presented in section 4.3.

3.5 Additive Layer Manufacture of Concept Car Models

To determine the ALM process best suited for use in the Virtual Wind Tunnel group project a matrix analysis was conducted, assessing important criteria for each method. The

ALM process selection and justification was initially presented in Browne [3]; a summary is provided below. The matrix analysis is displayed in Table 3 [3]. Because the concept car models were required to be small enough to fit into the University of Exeter wind tunnel, part size was omitted from the matrix criteria. It is however an important factor to consider when working with larger scale industrial models.

Table 3: Matrix analysis of ALM processes [3].

Process and Material	Surface Finish (/5)	Manufacture Lead Time (/5)	Cost (/5)	Geometrical Accuracy (/5)	Total (/20)
Laser Sintering – Nylon 12	2	3	2	2	9
Material Extrusion – ABS	3	4	3	3	13
Material Jetting – Acrylic	4	4	3	4	15

The material jetting process provided both the best surface finish and geometrical accuracy. Laser sintering had the lowest geometrical accuracy because the ‘flow’ of molten particulate materials lowers the dimensional tolerance. The lowest material costs were for the laser sintering process, however it also incurred the greatest manufacturing cost, making it more suited to batch production rather than one-off. Material jetting and extrusion both required expensive materials but were more cost effective for the one-off nature of production for custom automotive models. Laser sintering also had the quickest manufacturing time, however extra time was required for the part to heat up and cool down owing to the thermal nature of the process. Jetting and extrusion were therefore faster processes overall. It was concluded from the matrix analysis that material jetting was the method most suited for use in the Virtual Wind Tunnel group project due to the high quality surface finish, geometrical accuracy and relative cost effectiveness [3].

A specification from the Experimental sub-group was that the frontal face area of the scale model should not exceed 10% of the cross-sectional area of the wind tunnel test section. This was to ensure that wall effects, such as the formation of boundary layers, did not affect the flow around the car. Due to the limited size of the wind tunnel this would have resulted in an impractically small model (a total of length approximately 83mm), and would therefore make it difficult to take accurate readings due to the size of the testing apparatus. The concept car was scaled up appropriately, resulting in an overall length of 165mm. Another specification was that the final concept model should be able to move forwards and backwards with as little friction as possible, allowing the aerodynamic forces acting on it to be determined using a drag balance. It was decided that the model should be mounted on bearings located where the wheels would usually be. This fulfilled the requirement for minimum friction and provided a more realistic looking car model.

To assess the suitability of the model surface finish for wind tunnel testing the boundary layer thickness (introduced in section 2.1) was calculated. A surface can be said to be hydraulically smooth if the asperities fit within the laminar sub-layer [5]. The top of the car was assumed to behave like a flat plate immersed in a fluid flow. The thickness of the laminar boundary sub-layer at the point of transitional flow (where the Reynolds number equalled 10^5) was determined using Equation 1 and Equation 2 from section 2.1.

4. Results and Discussion

4.1 Concept Car Analysis

4.1.1 Modified Ahmed Body

The rear slant angle of the modified Ahmed body was varied to observe the effects on the drag. To suitably compare the flow patterns around the vehicle body for different rear slant angles velocity streamlines along the central plane were plotted. Figure 18 provides plots of the velocity streamlines for each slant angle. These diagrams are useful for highlighting the boundary layer separation and attachment.

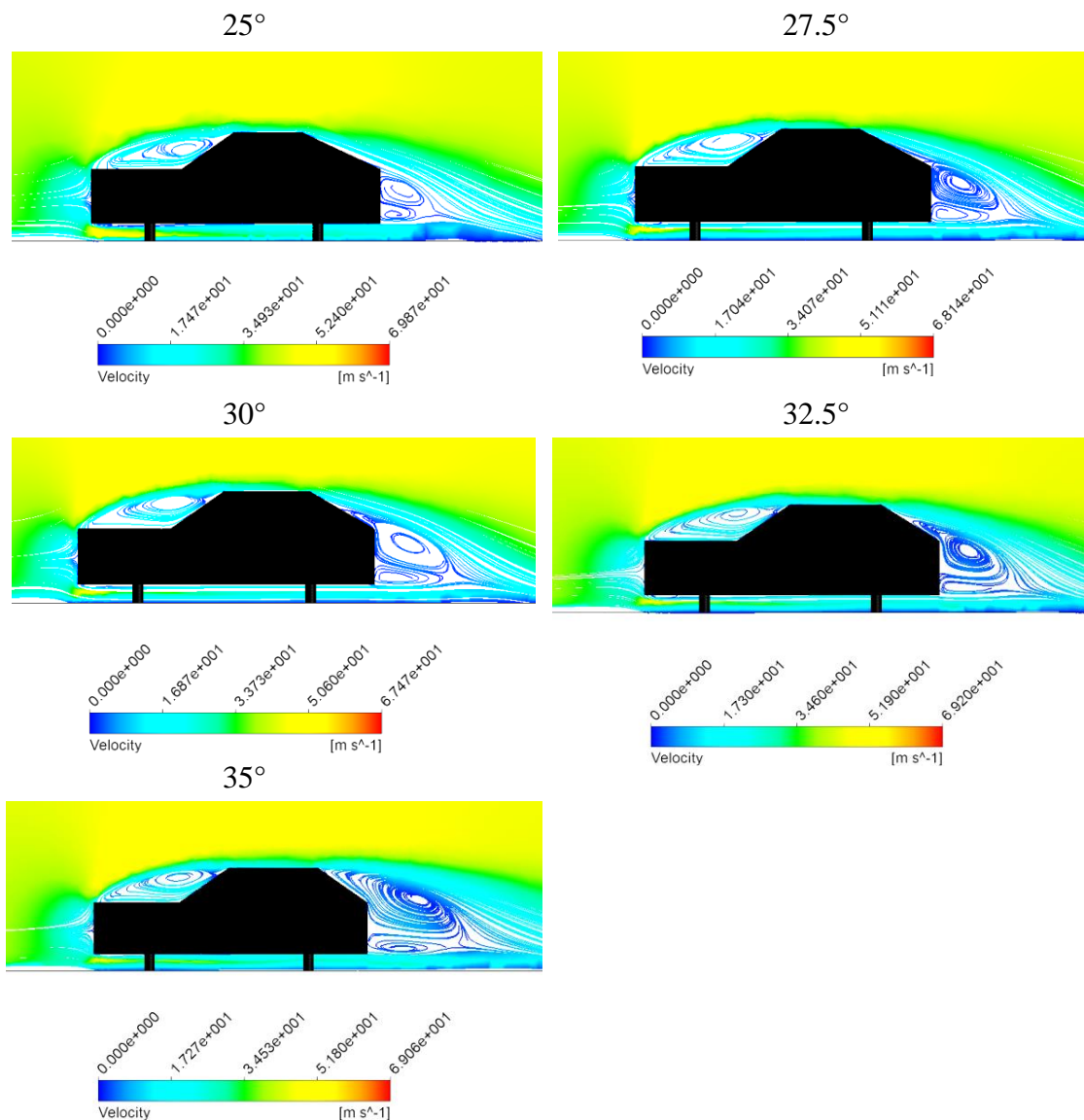


Figure 18: Velocity streamline plots for the modified Ahmed body.

In a study by Frank et al. [11] it was determined that the Ahmed body has two critical rear slant angles: 12.5 and 30 degrees. Maximum drag occurred at 30 degrees, corresponding to partially detached flow. Figure 19 [11] presents a diagram of the fluid flow around the rear of an Ahmed body for different slant angles. Diagrams I and II are slants below the first

critical angle, III is between the two critical angles and IV is greater than the second critical angle.

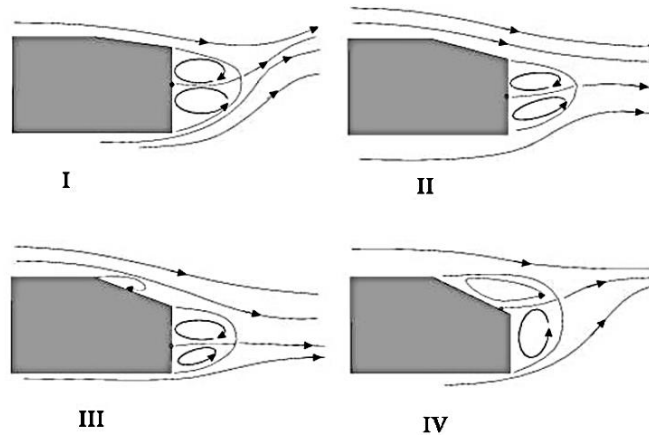


Figure 19: Diagrams of the flow behind the Ahmed body rear slant [11].

These diagrams present similar flow patterns to the velocity streamline plots provided in Figure 18, where the 25 and 27.5 degree slants show the formation of two vortices just behind the rear vertical face of the body. Diagram IV in Figure 19 also validates the flow behaviour shown by the modified Ahmed body with angles of 30 to 35 degrees, where the vortices increase in size and move vertically upwards to just behind the rear slant, corresponding to detached flow. Figure 20 provides a graph of the rear slant angle against the drag coefficient for the modified Ahmed body analysis.

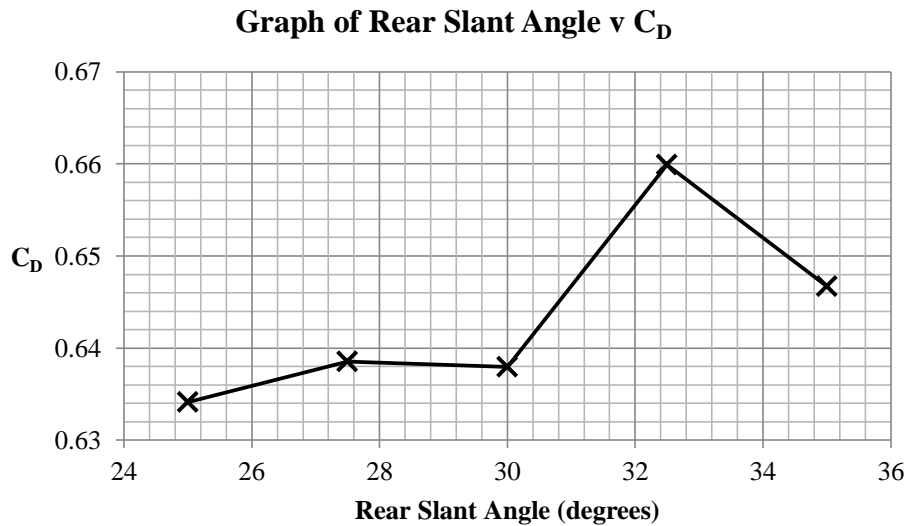


Figure 20: Graph of the rear slant angle against the drag.

The results provided in Figure 20 show that the maximum drag occurs at an angle of 32.5 degrees rather than 30 degrees, and corresponds to the separation of the boundary layer. The difference in results is partially a result of the inclusion of a bonnet to the Ahmed body, which leads to the formation of a vortex just before the ‘windscreen’. Another reason could derive from the numerical methods used; this project utilised a RANS turbulence model (realizable $k-\epsilon$), which has difficulty predicting flow separation.

4.1.2 Initial Concept Analysis

RANS CFD analysis of the initial concept car (derived from the modified Ahmed body) was conducted using the realizable $k-\epsilon$ turbulence model. Figure 21 displays the velocity streamline plot along the central plane of symmetry for the initial concept car.

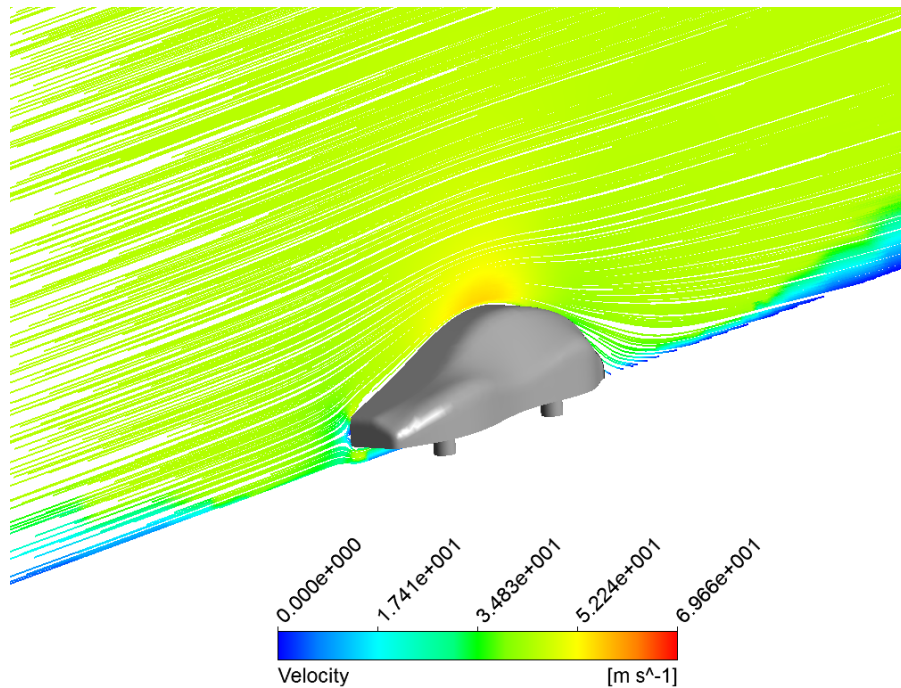


Figure 21: Velocity streamlines around the initial concept car along the symmetry plane.

The body profile was designed to incorporate a rear angle of approximately 25 degrees, a shallow windscreen angle and to have no sharp corners. From the simulation it was determined that the drag coefficient was equal to 0.32 – much lower than the drag coefficient of the modified Ahmed body (0.63 with a rear slant angle of 25 degrees).

4.1.3 Final Concept Analysis

The final concept car CAD model, which includes wheels, wing mirrors and a rear diffuser, is displayed in Figure 22. The final concept was modelled with the standard $k-\epsilon$, realizable $k-\epsilon$, SST $k-\omega$ and Spalart-Allmaras turbulence models. Figure 23 displays the velocity streamlines along the central plane of symmetry for the realizable $k-\epsilon$ model.

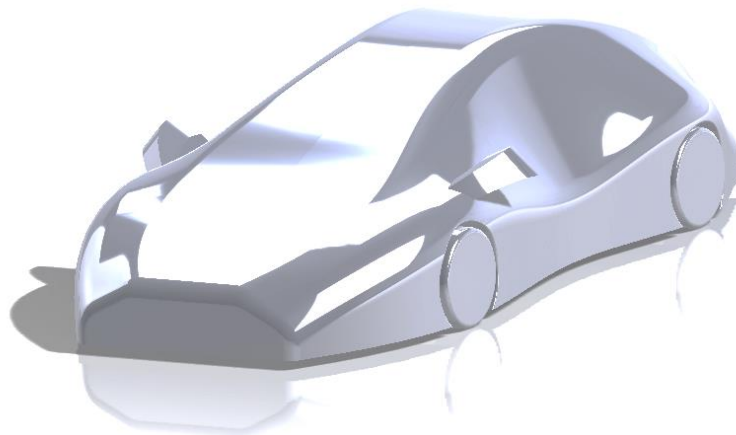


Figure 22: CAD model of the final concept car.

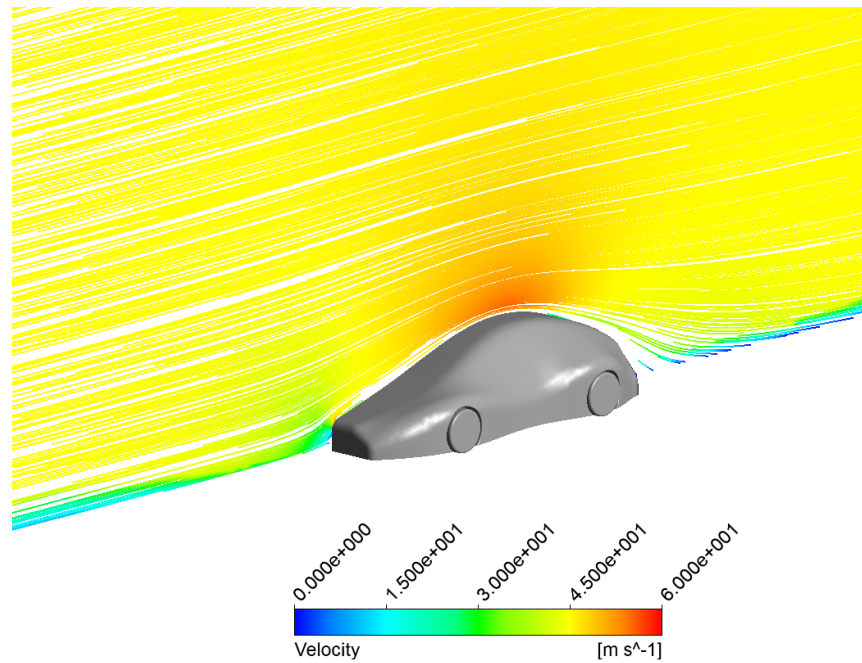


Figure 23: Velocity streamlines around final concept along the symmetry plane.

As expected an area of low velocity exists at the nose of the vehicle (the stagnation point), and the flow is accelerated as it passes over the curved roof. The areas of low velocity just above the surface of the simulated road correspond to a boundary layer. This only exists when air is moving over a stationary road surface, and is therefore unrealistic when considering a car moving into still air. The drag coefficient was concluded to equal 0.28; 0.04 less than the initial concept design. This is mainly because the car is positioned significantly lower to the road, resulting in less flow beneath the body. A comparison of the turbulence models and their outputs is discussed in the proceeding section.

4.1.3.1 Comparison of RANS Turbulence Models

The bar chart in Figure 24 highlights the difference between the lift and drag coefficients determined by the various RANS turbulence models used to analyse the final concept car.

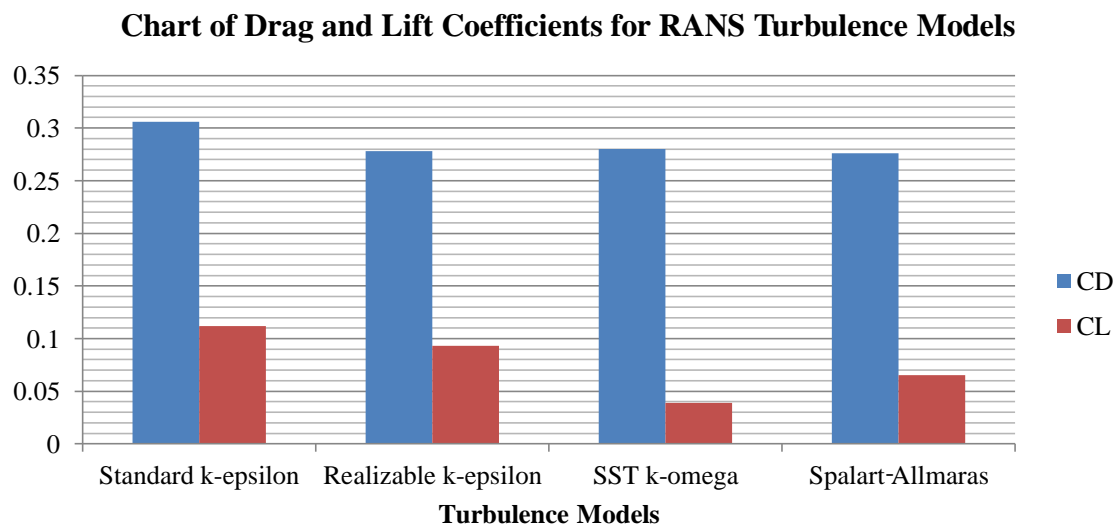


Figure 24: Comparison of drag (C_D) and lift (C_L) coefficients for different turbulence models.

The maximum change in C_D is of 9.8% between the standard $k-\epsilon$ and Spalart-Allmaras models, whilst minimal difference was observed between the realizable $k-\epsilon$, SST $k-\omega$ and Spalart-Allmaras models. The standard $k-\epsilon$ is said to perform poorly for unconfined flows with separation and large wakes [7], therefore it is likely that the results are less accurate compared to the other three models. Also, the Spalart-Allmaras model has been found to struggle when predicting flow reattachment around the rear of an Ahmed body [10]. It was therefore concluded that the realizable $k-\epsilon$ and SST $k-\omega$ models were most suited to automotive analysis due to their ability to better model flow separation, attachment and adverse pressure gradients, as described in section 2.2.1. The lift coefficients, although not strictly relevant to the project, have been included for comparison purposes, and show relatively large variations with each turbulence model.

4.1.3.2 Comparison between Uniform and Parabolic Inlet Velocity Profiles

A comparison between a uniform and parabolic inlet velocity flow case is given in Figure 25, which presents the velocity streamlines. The drag forces were calculated to equal 10.9N and 14.5N for the uniform and parabolic flow cases respectively. From the streamline plots it is clear that the parabolic inlet velocity condition produces a trail of vortices behind the concept car. The increased turbulence in the wake results in a larger pressure difference across the vehicle, therefore producing a greater drag force.

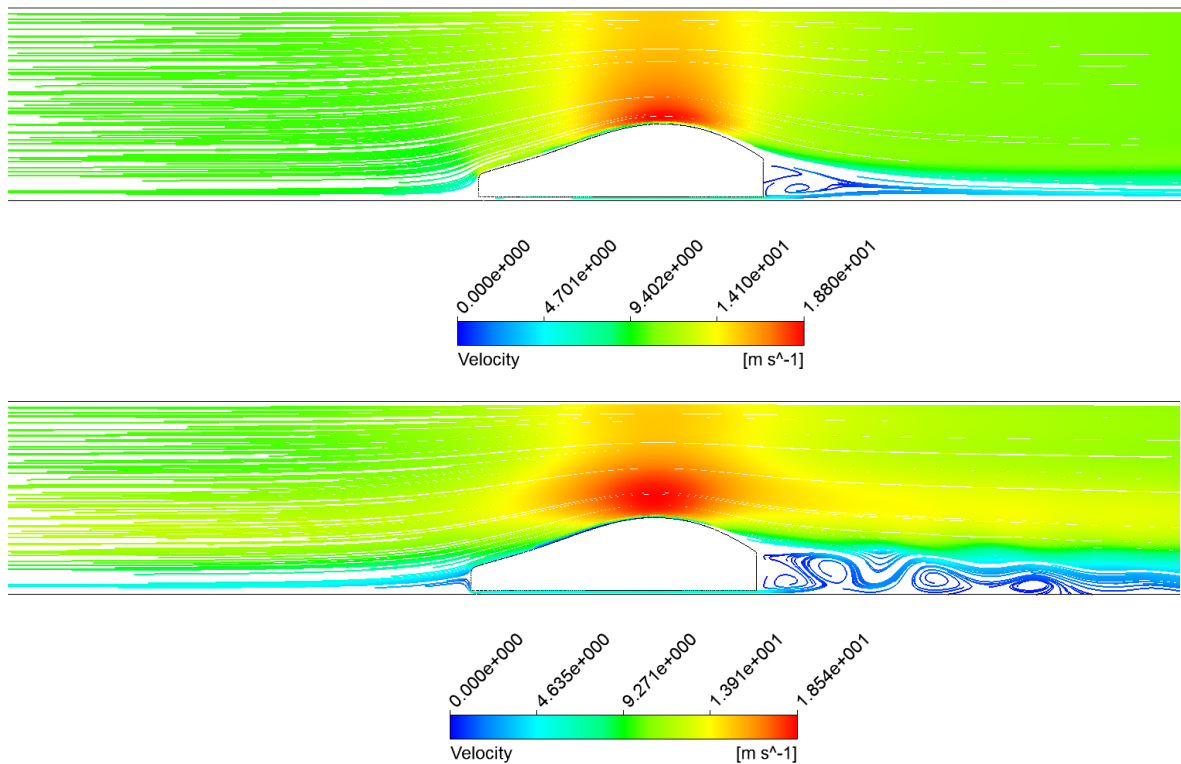


Figure 25: Velocity streamlines plots for uniform (top) and parabolic (bottom) inlet velocity cases.

Determining the fluid behaviour over a concept car under real-world flow conditions is an important part of the design process. Ideally a three-dimensional polynomial equation describing the velocity flow profile through an urban environment would have been applied. A larger flow domain would have also provided more realistic results.

4.2 Parametric Finite Element Analysis Study

This section provides the results of the parametric FEA design study conducted using SolidWorks. Figure 26 displays a graph of the displacement and mass against shell thickness. It can be seen that the mass relates approximately linearly to the shell thickness. On the other hand the rate of change of displacement decreases as the shell thickness increases.

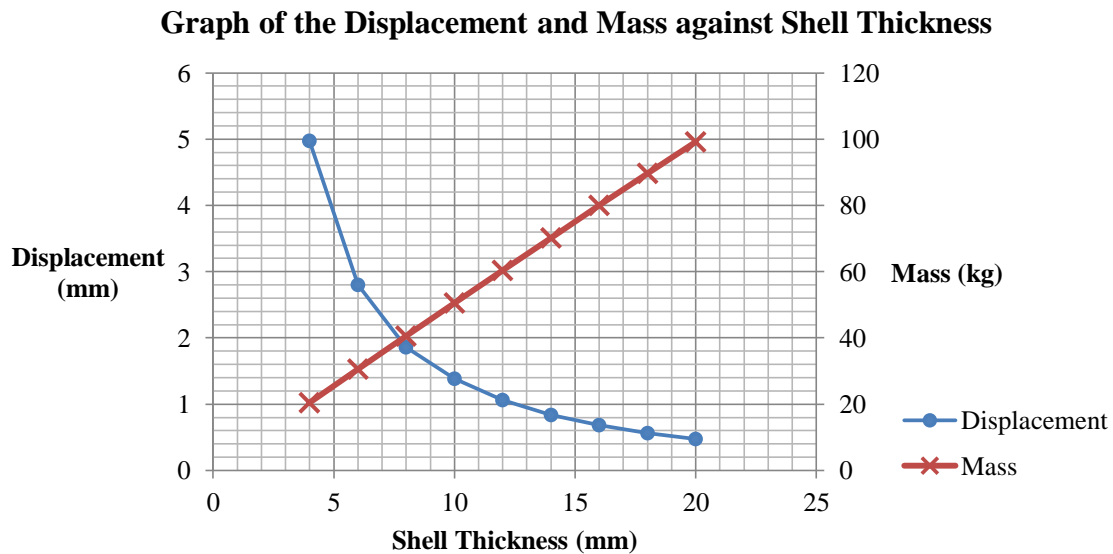


Figure 26: Graphs of displacement and mass against shell thickness from the parametric design study.

For the model to be commercially viable a compromise must be achieved between the maximum deflection and the mass of the model (which determines the manufacturing lead time and cost). For example, a deflection of 0.5mm will be more accurate when testing in the wind tunnel; however it corresponds to a mass of 100kg. On the other hand, if a displacement of 2mm was acceptable approximately 60kg of mass would be saved, resulting in a cheaper model with a significant reduction in manufacturing time. It was concluded that a shell thickness of 8mm provided a good compromise between mass and deflection, and was therefore subsequently used for the FSI analysis. Figure 27 shows the deflection plots for a model with a shell thickness of 8mm. As expected, the legs and the areas of the car body directly around them deflected minimally. The maximum deflection had a value of 1.87mm, located in the centre of the bonnet area on the vehicle.

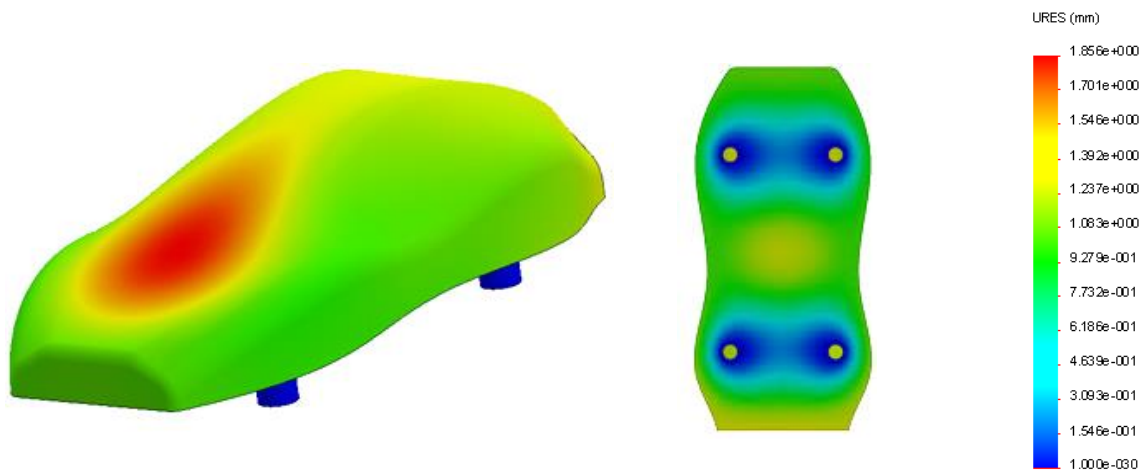


Figure 27: Plot of the overall deflection.

Figure 28 provides a plot of the Von Mises stress on the bottom of the car model. The underside of the car is the only view displayed because the rest of the body was subjected to minimal stress.

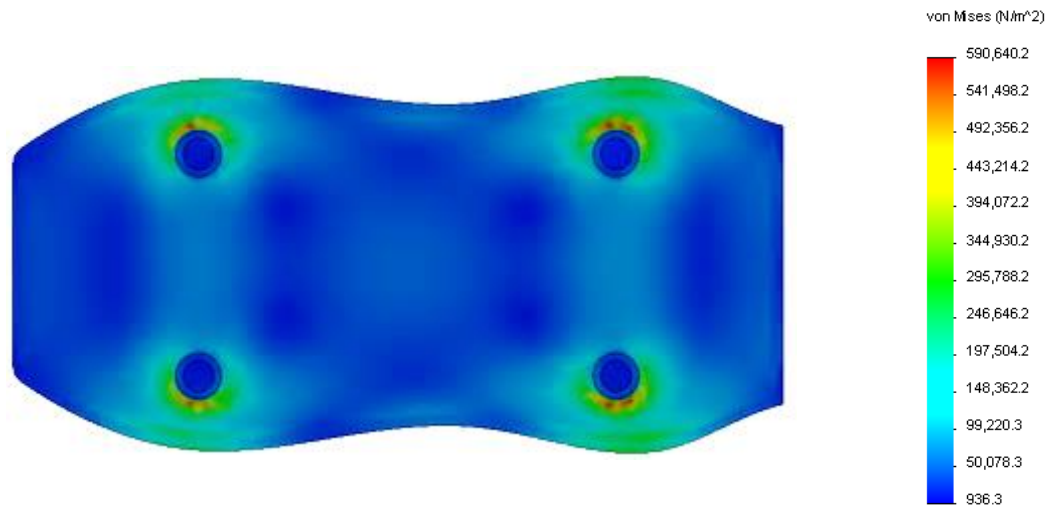


Figure 28: Plot of the Von Mises stress for the underside of the car body.

It can be seen that stress concentrations form between the legs and the body; a result of the sharp corners. The maximum stress reached a value of 590kPa, which was well below the tensile strength of acrylic (42.4MPa). It was therefore concluded that a 1:2 scale acrylic model with a shell thickness of 8mm would not fail or deform excessively under its own weight.

4.3 Fluid-Structure Interaction Analysis

The FSI analysis involved simulating a car model (at a scale of 1:2 and a shell thickness of 8mm) subjected to an aerodynamic pressure load. Figure 29 provides the plot of the pressure load on the car body. The maximum pressure was 2.64kPa, located at the outer side of the front leg.

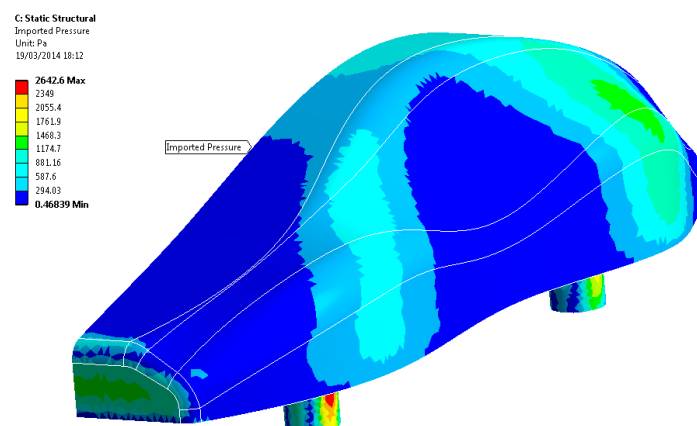


Figure 29: Plot of the pressure load on the car body.

The plots in Figure 30 show the Von Mises stresses on the car body as a result of the aerodynamic pressure load. Most of the car body was under very little stress, typically in the region of 2.45kPa, however this rose to a maximum of 7.92MPa at a stress concentration in the rear leg. This was due to a sharp corner present at a high pressure region.

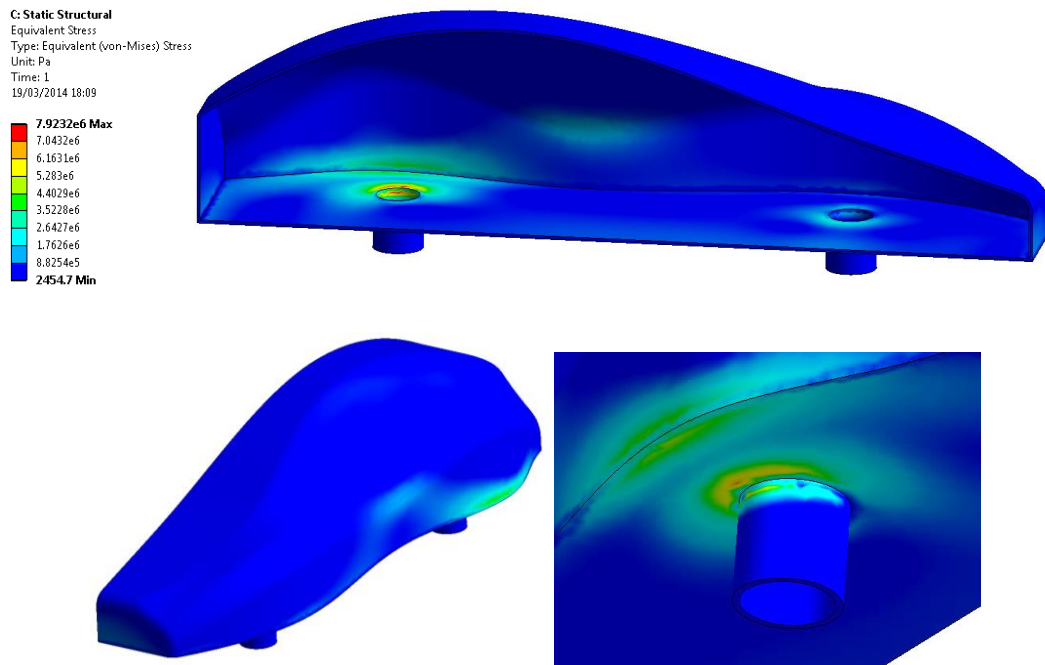


Figure 30: Von Mises stress plots for the car body under aerodynamic loading.

Figure 31 provides the plots of the overall deflection for the car body under aerodynamic loading. It can be seen that the maximum displacement (a value of 0.0107m) was located at the rear of the car body, due to the air being accelerated downwards after passing over the roof. This was a relatively small displacement for a model 2m in length, however it could still be great enough to have an adverse impact upon experimental results.

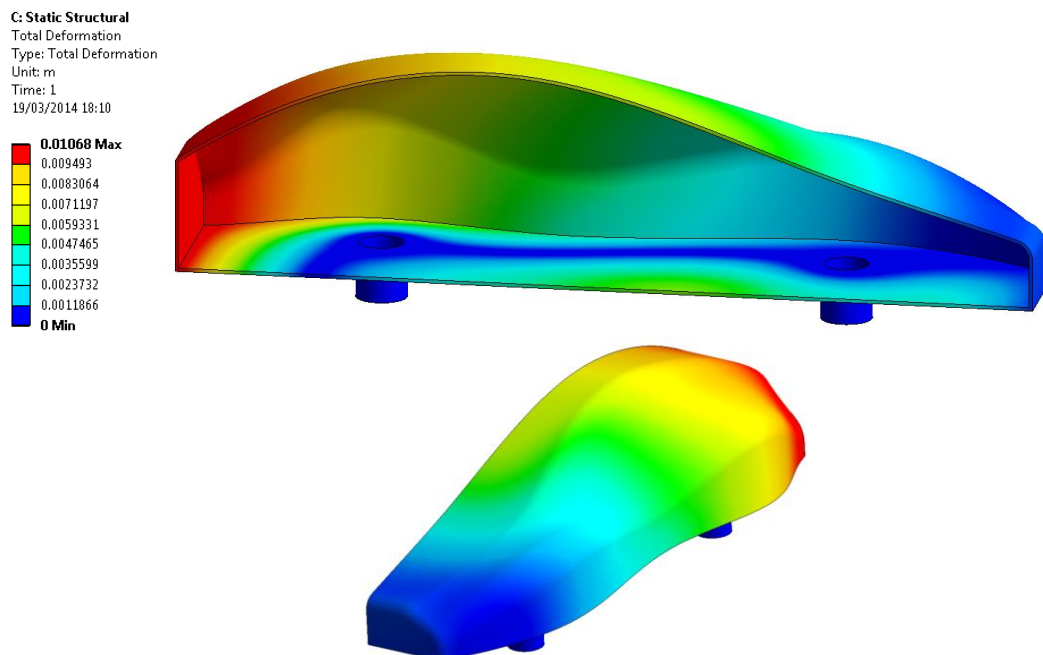


Figure 31: Deflection plots for the car body under aerodynamic loading.

To conclude, the aerodynamic pressure loads a model is subjected to in wind tunnels must be taken into account when producing scale models to ensure minimal deformation during testing. For an optimum high strength and low mass design a truss structure could be

directly manufactured into the hollow interior of the model, providing additional support to the areas identified to deflect most. This reflects one of the advantages of ALM, where integrated support structures can be introduced without adding to the complexity of the manufacturing process.

4.4 Additive Layer Manufacture of Scale Models

This section presents the results of the ALM scale models. Figure 32 shows a picture of the initial and final concept car models. The final model includes the bearings required for the experimental drag balance testing. Figure 33 presents close up photographs of various details on the final concept model.

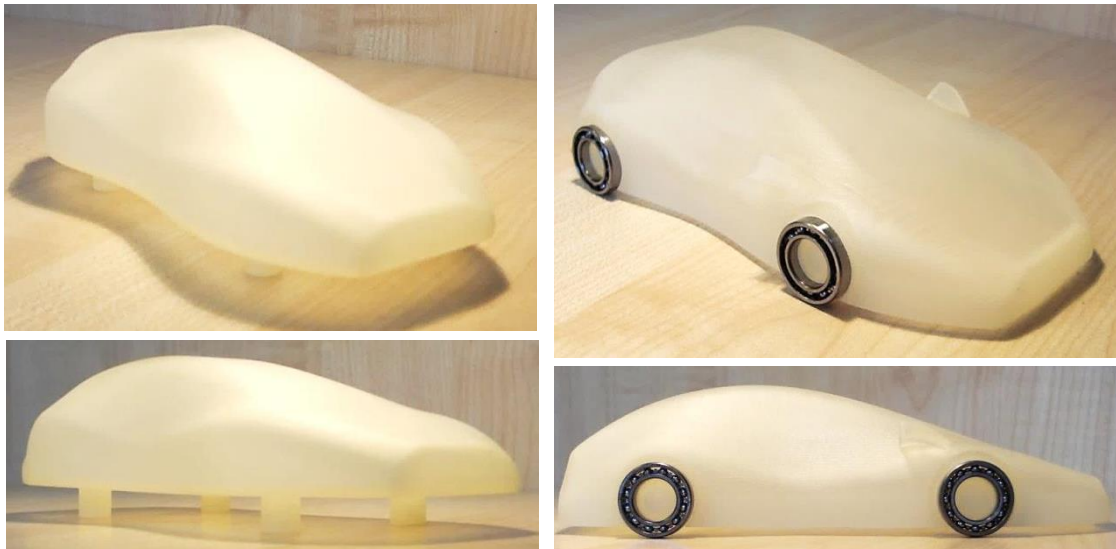


Figure 32: Photographs of the initial (left) and final (right) concept car ALM models.

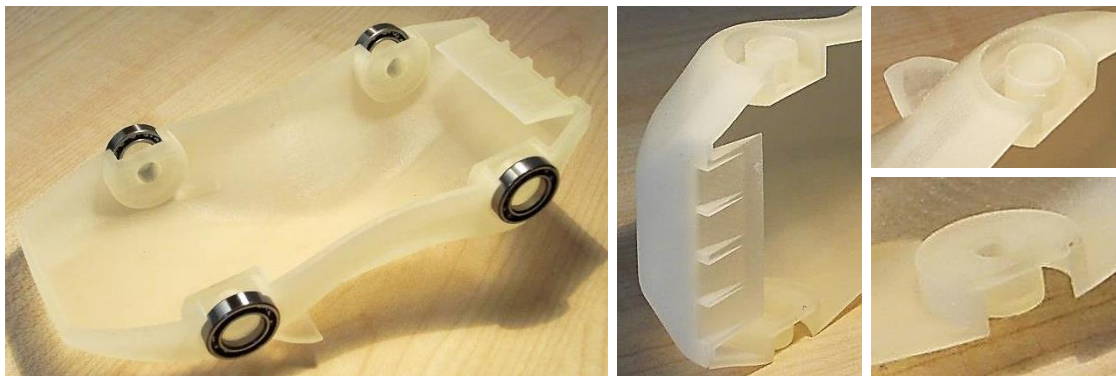


Figure 33: Photographs of the final concept car ALM model details.

Although the material jetting technique employed to manufacture the models provided the best finish available, the surface was still relatively rough in places. A very rough finish could potentially increase the size of the boundary layer and therefore the skin friction drag, introducing inaccuracies into the experimental results. By assuming that the top of the car behaved like an immersed flat plate of total length 165mm the boundary layer was determined to transition from laminar to turbulent flow at a length of 33.3mm from the leading edge (as described in section 3.5). The thickness of the laminar sub-layer at this point was calculated to equal 1.25mm. The maximum height of the asperities on the ALM model was estimated to be no more than 1mm, therefore the surface could be said to be hydraulically smooth, requiring no subsequent finishing processes.

If the surface was found not to be hydraulically smooth, models could be sanded by hand using fine glass paper, ensuring that a minimal amount of material was removed so as not to alter the geometry. Other techniques could be employed to obtain a smooth finish, such as spray painting or varnishing. For larger models, for example scale 1:2, the relative roughness would be lower, and would therefore require less post-processing. The models in the Virtual Wind Tunnel project were sanded by hand to provide the best possible finish for wind tunnel testing.

As described in section 2.6.1, automotive clay models are often formed on top of an existing chassis structure. A chassis with freely rotating wheels is necessary both to produce a realistic model and to allow it to be tested by a drag balance in the wind tunnel. This technique could also be implemented into the ALM model production process by creating a generic chassis acting as a base for the car body shell. This method would only require a shell of the car body to be secured on top of the chassis, resulting in simpler geometries, reduced material usage and shortened manufacturing times. Considerations regarding the positioning of the wheels must also be taken into account. To increase the design freedom and flexibility the wheels and axles should be fully adjustable. Another factor is the method of securing the model shell to the chassis. A proposed method is to produce and align holes in both the ALM model and chassis. The two surfaces can then be bolted together, allowing the assembly to be taken apart without damaging the individual parts. A diagram of an example chassis design is provided in Figure 34.

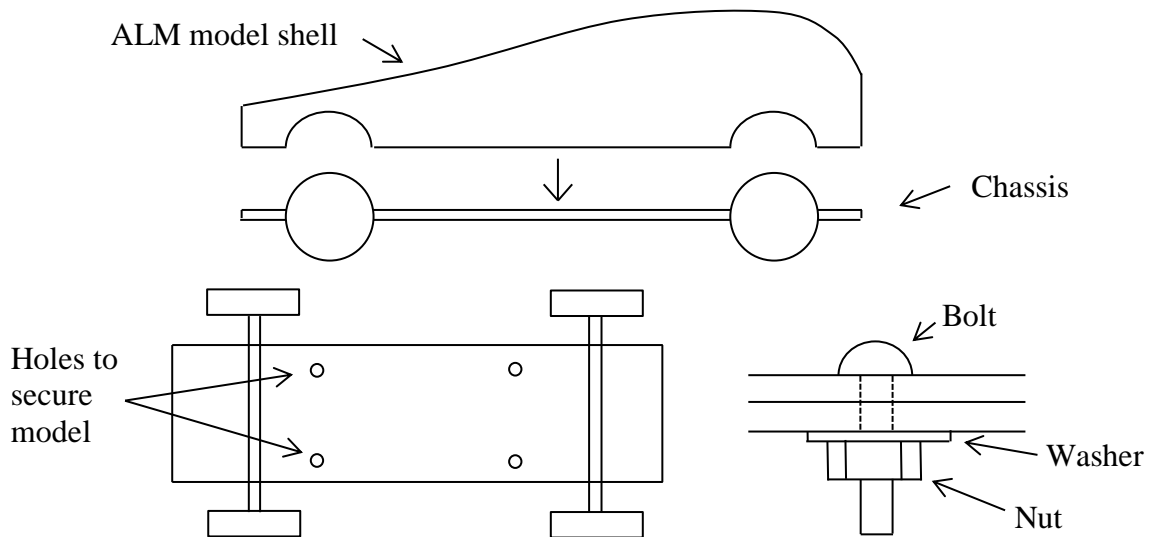


Figure 34: Diagram of an example chassis for ALM concept car models.

4.4.1 Comparison of ALM with Clay Modelling

Before ALM can be introduced into industrial design processes a number of criteria must be assessed. Table 4 provides a comparison between clay modelling and ALM techniques for the production of concept car models. The environmental aspects are omitted from the table and discussed in section 5.

Table 4: Summary of the comparison between clay modelling and ALM scale models.

Criteria	Clay Modelling	ALM
Surface finish	Clay can provide very good surface finishes because it is a soft, easily worked material.	The smoothness of a surface produced by ALM is limited by the layer thickness (dependent on the process). Polymer ALM models can be easily smoothed by sanding.
Scale	Clay models can be produced at virtually any scale, because it is simply applied to a pre-fabricated form such as foam.	The scale of ALM models is limited by the size of the equipment. Theoretically an ALM rig of almost any proportions can be specifically manufactured.
Ease of manufacture	Clay modelling requires highly skilled labourers to ensure that the car model is geometrically precise.	Scale models can be very easily produced using additive manufacture because it is an automated process. A CAD model can be simply updated, converted to an STL file (or similar) and printed with minimal further human input.
Adjustability	Clay models have the advantage that they can be continuously edited, by applying additional layers of clay, to reflect design updates.	Models produced by ALM are fixed and cannot be easily changed, other than surface processing such as sanding. This could result in the production of multiple models per project.
Detail	A high level of detail can be applied to clay models because the workers have complete control over the clay. It would however be difficult to create model with internal geometries.	ALM has the advantage of near complete geometrical freedom. A specific application is internal flow analysis, for example an engine inlet manifold. The internal geometry could be accurately created without the need for further processing. Space for testing equipment, for example channels for pitot tubes, can also be directly manufactured without adding to the overall complexity.
Manufacture lead times	Clay modelling is a process requiring numerous different stages (from manufacturing the pre-form to surface finishing), and therefore involves relatively long lead times.	Although the additive manufacture of a large scale automotive model could take several days, it is still more rapid than clay modelling. In the long term it has the potential to be a very time and cost effective alternative.
Cost	Clay modelling is advantageous in that less expensive equipment is required compared to ALM, because the models are produced by hand using a relatively inexpensive material. A disadvantage however is that skilled labourers must be continuously employed and given adequate training.	ALM requires a large initial investment to provide the necessary equipment, however once it has been purchased very little human input is required during production. Also, the savings from clay modellers' salaries and the reduction in project lead times are likely to produce financial rewards in the long term.

5. Sustainability

This section discusses the sustainability issues associated with the Virtual Wind Tunnel project, focussing on the introduction of ALM into the automotive design process. Three major areas of sustainability concern were identified to be social, environmental and economic impacts.

Regarding the social impacts of ALM the creation of physical clay models is a skilled job, and the integration of CAD and automated ALM processes could lead to machines replacing the current human labour force. A wide range of environmental impacts must also be considered. A general aim of the group project was to improve the automotive design process, of which a major industry target is to reduce aerodynamic drag aiming to improve fuel consumption [1]. This is a key goal due to the requirement for more efficient vehicles to comply with new industry standards and regulations. Specifically, the target fleet average of CO₂ to be produced by cars is 130 grams per kilometre by 2015 [1].

Material waste in ALM processes is dramatically reduced compared to subtractive machining techniques, because 95% to 98% of waste powder can be recovered and recycled [60]. A main issue relating to ALM model construction is the recycling of the scale models after experimental testing. Ideally the material should be fully recyclable, for example thermoplastics such as acrylic and nylon, allowing the polymer construct to be processed and re-used for a later model. This is a disadvantage compared to clay, which can be relatively easily removed and re-used. As stated in Table 4, clay models can also be continually updated and modified without the need to start from scratch. On the other hand, if an ALM model was found to be incorrect or contain imperfections an entire new part would need to be made, potentially contributing to landfill waste. Figure 35 [61] displays a graph of the waste going to landfill in the automotive sector.

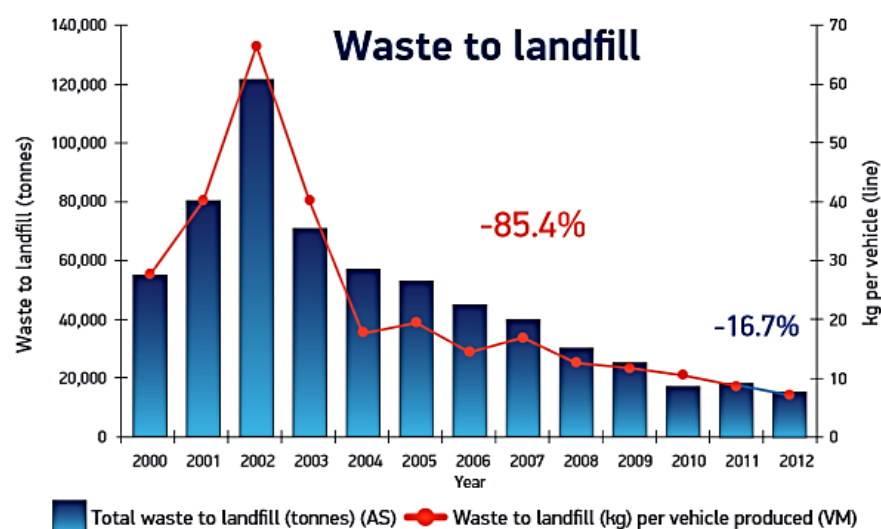


Figure 35: Graph of the waste to landfill per car produced [61].

The energy consumption of industrial processes, for example additive manufacture, has both environmental and economic impacts. ALM is generally a very energy intensive process, resulting in high utility costs and therefore less environmentally friendly production. Table 5 [62] compares the energy consumption rate of three ALM processes.

Table 5: Comparison of energy consumption per kg for ALM processes [62].

ALM Process	Energy Consumption Rate (kW h/kg)
Stereolithography	20.70 – 41.38
Laser Sintering	29.83 – 40.09
Fused Deposition Modelling	23.08 – 346.4

Clay modelling on the other hand requires little energy; however it is a long and labour intensive method requiring the employment of skilled workers for relatively long periods of time. Continuing the theme from the ‘cost’ criteria in Table 4, a Return on Investment analysis should be conducted in order to determine the long term investment value of the large initial equipment costs of ALM machinery and the savings obtained per project. This could then be compared to the cost of employing clay modellers and the financial implications of longer project lead times. Figure 36 [61] describes the trend of energy consumption during automotive production from the years 2000 to 2012.

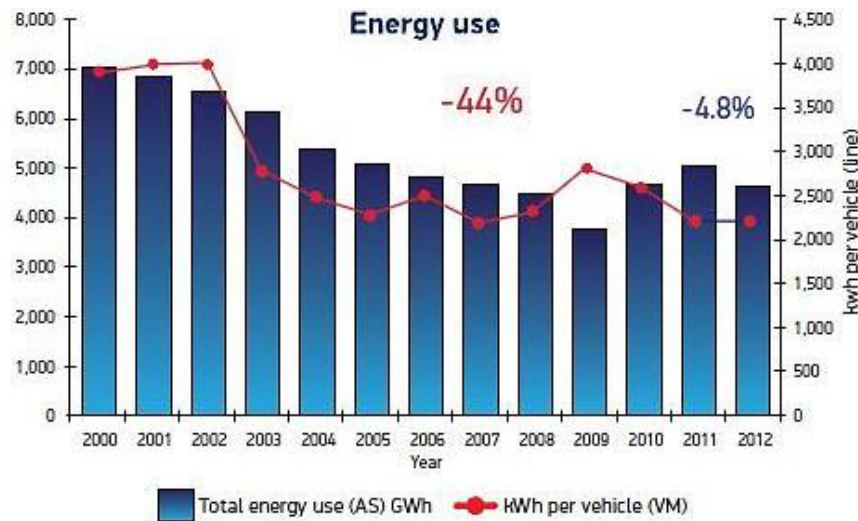


Figure 36: Graph of the automotive production energy consumption [61].

Regarding numerical analysis, a major reason for the running of computational simulations is to limit the need for experimental testing, therefore saving both materials used for manufacturing the scale models and reducing the high energy costs associated with running an industrial wind tunnel. Theoretically, if CFD models were completely accurate experimental testing would not be required, therefore the only costs involved would be initial hardware and software expenses and energy consumption.

Overall, ALM would have a worse environmental and social impact than clay modelling due to the loss of skilled jobs, energy intensive methods and potentially increased landfill waste. These factors would need to be addressed before ALM could be successfully integrated into industry.

6. Project Management

The Virtual Wind Tunnel project was managed in several different ways. A meeting of the entire group was held on a weekly basis to discuss progress and the future direction of the project, encouraging group cohesion. An agenda was created prior to the meeting by the chair. The outcomes of the group meetings were recorded in a minutes book – the responsibility of which was that of the group secretary. The role of chair and secretary rotated each week throughout the entire group. Meetings between the Automotive Design sub-group were also held on a weekly basis to collaborate results and provide regular constructive feedback. An individual project logbook was kept up to date in order to record and process all ideas and work relevant to the project.

Work and research resources were uploaded to an online, cloud-based storage space. Documents could therefore be effectively shared with the group and accessed from any computer with an internet connection. Alongside this a group page was established on a social media site, allowing direct communication with the entire group.

The Gantt chart is a useful management tool for checking and updating project progress, because it shows task dependencies and the timescale for which they must be completed with respect to the whole project. An initial Gantt chart was created at the beginning of the project and updated regularly in order to reflect any developments or setbacks. The final Gantt chart is provided in Appendix B. Health and safety is also an important part of any project in order to mitigate risks and prevent injury. A risk assessment, provided in Appendix C, was therefore carried out based upon the University of Exeter and Health and Safety Executive risk assessment forms [63, 64].

6.1 Budgeting

The total budget for the group was £800 (£100 per person). Walton was assigned the responsibility of group Treasurer. The HPC group required very little of the budget, because most of their work involved numerical analysis using existing computational resources. The Experimental group on the other hand needed the majority of it for the purchase of materials and parts to construct the wind tunnel test section. The remaining portion of the budget, roughly estimated at £300, was assigned to the Automotive Design sub-group. The costs of the two concept car models were £120.15 and £126.92, resulting in a total cost of £247.07 – well within the allocated budget. The expenses can be further broken down into approximate costs of £400 per kilogram of material, and £8 to £10 per labour hour.

7. Conclusions

7.1 Summary

This report has detailed the work undertaken for the individual study completed as part of the Virtual Wind Tunnel group project. The aims of the project presented herein were to design a concept car, conduct RANS CFD analysis and produce two scale models using Additive Layer Manufacture. To summarise, a concept car was designed and numerically analysed using RANS turbulence models. The drag coefficient (a value 0.28 for the final concept car) was minimised by setting a rear slant angle of approximately 25 degrees, avoiding sharp corners and incorporating a shallow windscreen angle. It was concluded that the realizable k- ϵ and SST k- ω turbulence models were most suited to modelling external automotive aerodynamics because of their performance dealing with flow separation and attachment. From the analysis involving an urban environment velocity profile, it was determined that the highly turbulent wake caused by a parabolic inlet velocity increased the drag force.

The integration of ALM into the automotive design process was also explored. It was concluded that ALM is a feasible process to replace clay modelling in the automotive industry. A main reason for this is the relatively rapid production of a physical model direct from a CAD model, resulting in reduced project lead times. Also, the complete design freedom allows for complex scenarios such as internal flow analysis. Due to the high initial investments involved financial gains are likely to be long term. From the FEA and FSI analysis it was concluded that a compromise must be made between the required geometrical accuracy of a model when tested in a wind tunnel, the material costs and manufacturing lead times. Scale model structural strength could be increased by integrating an internal truss structure. The major disadvantages associated with the replacement of clay modelling with ALM include high initial investments and issues with sustainability.

7.2 Recommendations for Future Work

Several areas for future work have been identified. A specific area of study not undertaken in this project is the thermal behaviour of polymer ALM models in wind tunnels. The wide range of temperatures experienced in the testing environment could have a significant impact upon both mechanical properties and dimensional stability. Exploring alternative forms of 3D printing for model production is a suitable topic for further investigation. A new approach is to consider the production of metal parts using processes such as laser melting or wire extrusion. An ALM machine producing metal parts also has the potential to manufacture automotive components outside of concept car prototyping, for example engine components. The dual role could be more cost effective than a machine producing only polymer concept car models.

This report has also introduced the possibility of creating a generic chassis to provide a base for ALM model shells. The design of an efficient way to produce and mount models ready for testing could be explored, alongside the design of a chassis which allows the wheel and axle positioning to be adjusted. The overall goal of this would be to further reduce the project lead time. Regarding non-technical work, it has been suggested that a Return on Investment analysis is conducted exploring the various financial implications of ALM processing, equipment and material costs, in-house versus external manufacture, and the reduction in labour hours and project lead time. The outcome should be expressed as a financial saving per project, and assessed against the cost of implementing these new measures.

References

- [1] European Commission. *Reducing CO2 emissions from passenger cars*. Available Online: http://ec.europa.eu/clima/policies/transport/vehicles/cars/index_en.htm. Accessed: 16/04/2014
- [2] Browne, F., Hamilton, L., Nima, D., Blades, L., Docherty, D., Bolt, H., Walton, J., Crinion, E. (2013) "Group Report 1: Virtual Wind Tunnel Project", *MEng Report*, University of Exeter
- [3] Browne, F. (2013) "Individual Report 1: Virtual Wind Tunnel Project" *MEng Report*, University of Exeter
- [4] Acheson, D.J. *Elementary Fluid Mechanics*. 1st Edition, Oxford University Press. 1990
- [5] Douglas, J.F., Gasiorek, J.M., Swaffield, J.A., Jack, L.B. *Fluid Mechanics*. 6th Edition, Pearson, Harlow. 2011
- [6] Sayma, A. *Computational Fluid Dynamics*, Ventus Publishing. 2009
- [7] Versteeg, H.K., Malalasekera, W. *An Introduction to Computational Fluid Dynamics*. 2nd Edition, Prentice Hall, Harlow. 2007
- [8] Grant, S. (2002) "Development and Application of a New Wall Function for Complex Turbulent Flows" *PhD Thesis*, University of Manchester
- [9] Hoda, A. (2007) "Turbulence modeling for film cooling flows" *PhD Thesis*, Louisiana State University
- [10] Rajsinh, C., Raj, T. (2012) "Numerical Investigation of External Flow around the Ahmed Reference Body Using Computational Fluid Dynamics" *Research Journal of Recent Sciences*, 1(9), pp1-5
- [11] Franck, G., Nigro, N., Storti, M., D'Elia, J. (2009) "Numerical simulation of the flow around the Ahmed vehicle model" *Latin American Applied Research*, 39(4), pp295-306
- [12] Frohlich, J., von Terzi, D. (2008) "Hybrid LES/RANS methods for the simulation of turbulent flows" *Progress in Aerospace Sciences*, 44(5), pp349-377
- [13] Walters, D., Bhushan, S., Alam, M., Thompson, D. (2013) "Investigation of a Dynamic Hybrid RANS/LES Modelling Methodology for Finite-Volume CFD Simulations" *Flow Turbulence and Combustion*, 91(3), pp643-667
- [14] Fluent Inc., *Fluent 6.3 User's Guide*. 2006. Available Online: http://aerojet.engr.ucdavis.edu/fluenthelp/html/ug/main_pre.htm. Accessed: 11/04/2014
- [15] Ahmed, S., Ramm, G., Faltin, G. (1984) "Some salient features of the time averaged ground vehicle wake" *SAE Technical Paper*, 840300

- [16] Hinterberger, C., Garcia-Villalba, M., Rodi, W. (2004) "Large eddy simulation of flow around the Ahmed body" *The Aerodynamics of Heavy Vehicles: Trucks, Buses and Trains*, 19, pp77-87
- [17] Liu, Y., Moser, A. (2003) "Numerical modeling of airflow over the Ahmed Body" *Proceedings of CFD*, 2, pp507-512
- [18] Franck, G., D'Elia, J. (2004) "CFD modeling of the flow around the Ahmed vehicle model" *In Proceedings of 2nd conference on advances and applications of GiD*
- [19] Hucho, W.-H. (1993) "Aerodynamics of Road Vehicles" *Annual Review of Fluid Mechanics*, 25, pp485-537
- [20] Minguez, M., Pasquetti, R., Serre, E. (2008) "High-order large-eddy simulation of flow over the "Ahmed body" car model" *Physics of Fluids*, 20(9), pp1-17
- [21] Kapadia, S., Roy, S., Vallero, M., Wurtzler, K., Forsythe, J. (2004) "Detached-Eddy Simulation Over a Reference Ahmed Body" *Direct and Large-Eddy Simulation V, Proceedings*, 9, pp481-488
- [22] Meile, W., Brenn, G., Reppenhagen, A., Lechner, B., Fuchs, A. (2011) "Experiments and numerical simulations on the aerodynamics of the Ahmed body" *CFD Letters*, 3(1), pp32-39
- [23] Saqr, K., Musa, M. (2010) "RANS Simulation of the Turbulent Flow Field in the Vicinity of the Ahmed Reference Car Model" *New Aspects of Fluid Mechanics, Heat Transfer and Environment*, 8th International Conference, pp21-26
- [24] Bayraktar, D., Landman, D., Baysal, O. (2001) "Experimental and computational investigation of Ahmed body for ground vehicle aerodynamics" *SAE Technical Paper*, 2001-01-2742
- [25] Lienhart, H., Stoots, C., Becker, S. (2002) "Flow and Turbulence Structures in the Wake of a Simplified Car Model" *New Results in Numerical and Experimental Fluid Mechanics III*, 77, pp323-330
- [26] Ramamurty, G. *Applied Finite Element Analysis*. Second Edition, L.K. International Publishing House Pvt. Ltd. 2010
- [27] Henwood, D., Bonet, J. *Finite Elements: A Gentle Introduction*. First Edition, Macmillan Press Ltd. 1996
- [28] Souli, M., Mahmadi, K., Aquelet, N. (2004) "ALE and Fluid Structure Interaction" *Materials Science Forum Volumes*, 465-466, pp143-150
- [29] Krawczyk, P., Beyene, A., MacPhee, D. (2013) "Fluid structure interaction of a morphed wind turbine blade" *International Journal of Energy Research*, 37(14), pp1784-1793

- [30] Hou, G., Wang, J., Layton, A. (2012) "Numerical Methods for Fluid-Structure Interaction – A Review" *Communications in Computational Physics*, 12(2), pp337-377
- [31] Sotiropoulos, F., Yang, X. (2014) "Immersed boundary methods for simulating fluid-structure interaction" *Progress in Aerospace Sciences*, 65(1), pp1-21
- [32] Gil, A.J., Arranz Carreno, A., Bonet, J., Hassan, O. (2013) "An enhanced Immersed Structural Potential Method for fluid-structure interaction" *Journal of Computational Physics*, 250, pp178-205
- [33] Hesch, C., Gil, A.J., Arranz Carreno, A., Bonet, J. (2012) "On continuum immersed strategies for Fluid-Structure Interaction" *Computer Methods in Applied Mechanics and Engineering*, 247(5), pp51-64
- [34] Gaylard, A. 2014. *Discussion on automotive design processes*. [Personal communication 06/03/2014]
- [35] Gibson, I., Rosen, D.W., Stucker, B. *Additive Manufacturing Technologies Rapid Prototyping to Direct Digital Manufacturing*. Springer. ISBN: 978-1-4419-1119-3. 2010
- [36] Fadel, G.M., Kirschman, C. (1996) "Accuracy issues in CAD to RP translations" *Rapid Prototyping Journal*, 2(2), pp4-17
- [37] Bianconi, F. (2002) "Bridging the gap between CAD and CAE using STL files" *International Journal of CAD/CAM*, 2(1), pp55-67
- [38] Wang, W.C., Gu, H.X. (2011) "Direct Slicing of CAD Model and Volumetric Error Compensation in Rapid Prototyping" *Advanced Materials Research*, 317-319, pp1598-1602
- [39] Jamieson, R., Hacker, H. (1995) "Direct slicing of CAD models for rapid prototyping" *Rapid Prototyping Journal*, 1(2), pp4-12
- [40] Kalpakjian, S., Schmid, S.R. *Manufacturing Engineering and Technology*. 4th Edition, Prentice Hall. 2001
- [41] Pham, D.T., Gault, R.S. (1998) "A comparison of rapid prototyping technologies" *International Journal of Machine Tools & Manufacture*, 38(10-11), pp1257-1287
- [42] Yang, Y, Li, S., Zhang, R., Lin, F., Wu, R., Lu, Q., Xiong, Z., Wang, X. (2009) "Rapid Prototyping and Manufacturing Technology: Principle, Representative Technics, Applications, and Development Trends" *Tsinghua Science and Technology*, 14(S1), pp1-12
- [43] Laser Prototypes Europe Ltd. Available Online: <http://www.laserproto.com/latest-news/dream-maker>. Accessed: 04/04/2014

- [44] 3ders.org. *3D printed car model DrivAer as a key to vehicle air circulation*. Available Online: <http://www.3ders.org/articles/20120907-3d-printed-car-model-drivaer-as-a-key-to-vehicle-air-circulation.html>. Accessed: 04/04/2014
- [45] Voxeljet AG, *VX4000: The large-format 3D printing system*. Available Online: <http://www.voxeljet.de/en/systems/vx4000/>. Last Accessed: 04/04/2014
- [46] Voxeljet AG, *Aston Martin Model*. Available Online: http://www.voxeljet.de/uploads/tx_sdreferences/pdf/plastic_model_Aston_Martin_ENG_2012.pdf. Accessed: 04/04/2014
- [47] 3D Print.Com, *China's Huge 3D Printers, Soon Able to Print Automobile Sized Metal Objects*. Available Online: <http://3dprint.com/733/chinas-huge-3d-printers-soon-able-to-print-automobile-sized-metal-objects/>. Accessed: 04/04/2014
- [48] Dassault Systèmes, Solidworks (Version 2014) [Computer program]
- [49] ANSYS, Inc., ANSYS FLUENT (Version 14.5) [Computer program]
- [50] Nima, D. (2014) "Individual Report 2: Virtual Wind Tunnel Project" *MEng Report*, University of Exeter
- [51] Crinion, E. (2014) "Individual Report 2: Virtual Wind Tunnel Project" *MEng Report*, University of Exeter
- [52] Walton, J. (2014) "Individual Report 2: Virtual Wind Tunnel Project" *MEng Report*, University of Exeter
- [53] Lanfrit, M. (2005) "Best practice guidelines for handling Automotive External Aerodynamics with FLUENT" Version 1.2, Fluent Deutschland GmbH
- [54] Al-Witry, A., Es-Saheb, M. (2013) "Benchmarking the Performance of the ANSYS-FLUENT Standard k- ϵ Turbulence Model in Fluid Flow and Heat Transfer Predictions for Complex Flows around Circular Pin-Fins Using Various near Wall Functions" *Research Journal of Applied Engineering Sciences, Engineering and Technology*, 5(17), pp4301-4310
- [55] Hamilton, L. (2014) "Individual Report 2: Virtual Wind Tunnel Project" *MEng Report*, University of Exeter
- [56] Fluent Inc., *A Step-by-Step UDF Example*, 2001. Available Online: http://combust.hit.edu.cn:8080/fluent/Fluent60_help/html/udf/node15.htm. Accessed: 18/04/2014
- [57] Three D Systems Circle. *Visijet Brochure*. 2010
- [58] e-Manufacturing Solutions, *PA 220 Balance 1.0*. Available Online: www.materialdatacenter.com. Accessed: 27/04/2014
- [59] Stratasys, *ABSplus Brochure*. 2007

- [60] Petrovic, V., Gonzalez, J.V.H., Ferrando, O.J., Gordillo, J.D., Puchades, J.R.B., Grinan, L.P. (2011) “Additive layered manufacturing sectors of industrial applications: shown through case studies” *International Journal of Production Research*, 49(4), pp1061-1079
- [61] The Society of Motor Manufacturers and Traders Limited, 2013 “2013 Automotive Sustainability Report, The 14th edition – 2012 data”. Available Online: <http://www.smmmt.co.uk/wp-content/uploads/sites/2/SMMT-Automotive-Sustainability-Report-2013.pdf>. Accessed: 16/04/2014
- [62] Baumann, M., Tuck, C., Bouurell, D.L., Sreenivasan, R., Hague, R. (2011) “Sustainability of additive manufacturing: measuring the energy consumption of the laser sintering process” *Proceedings of the Institution of Mechanical Engineers, Part B: Journal of Engineering Manufacture*, 225, pp2228-2239
- [63] University of Exeter Risk Assessment Form. Available Online: <http://www.exeter.ac.uk/staff/wellbeing/safety/formssignsandtemplates/>. Accessed: 18/04/2014.
- [64] Health and Safety Executive, *Example risk assessment for an office-based business*. Available Online: <http://www.hse.gov.uk/Risk/casestudies/index.htm>. Accessed: 18/04/2014

Appendix A: User Defined Function for a Parabolic Inlet Velocity Profile

```

/*****
*/
/* udf.c
*/
/* UDF for specifying a steady-state velocity profile boundary condition
*/
/*****
*/

#include "udf.h"

DEFINE_PROFILE(inlet_x_velocity, thread, index)
{
    real x[ND_ND];
    real y;
    face_t f;

    begin_f_loop(f, thread)
    {
        F_CENTROID(x, f, thread);
        y = x[1];
        F_PROFILE(f, thread, index) = (0.506*(y*y*y*y*y*y))-
(5.0841*(y*y*y*y*y))+(17.562*(y*y*y*y))-
(22.423*(y*y*y))+(0.0843*(y*y))+(16.885*y)+4.4157;
    }
    end_f_loop(f, thread)
}

```

Appendix B: Health and Safety Risk Assessment

Likelihood	Score (/5)	Severity	Score (/5)
Improbable	1	Very minor injury: abrasions/confusions	1
Remote	2	Minor Injuries: cuts/burns	2
Possible	3	Major injuries: fractures/cuts/burns/damage to internal organs	3
Probable	4	Severe injury: amputation/eye loss/permanent disability	4
Likely	5	Death	5

Hazard	Risk	Cause	Likelihood (L)	Severity (S)	Importance (LxS)	Action to minimise risk
Surrounding working environment (i.e. room).	Risk of slipping on wet floors, tripping over cables etc.	Untidy workplace, floor area not clear, equipment not properly stored.	3/5	2/5	6/25	Ensure all equipment such as cables are properly stored, mess and spillages are cleaned promptly etc.
Immediate working area (i.e. desk).	Risk of posture problems and discomfort whilst working including headaches, Repetitive Strain Injury etc.	Unsuitable lighting, poor seating and workstation layout, working at a computer for extended periods of time.	4/5	1/5	4/25	Ensure the workstation is suitable for use – comfortable chair; computer monitor is at the correct height, suitable room lighting etc. Take frequent breaks from work, drink enough water.
Sanding of ALM models.	Risk of polymer dust/particulates being inhaled or getting in the eyes.	Room not properly ventilated, protective eyewear not worn.	2/5	2/5	4/25	Ensure suitably ventilated work room is used, wear protective goggles.

Appendix C: Final Gantt Chart

